Early Cambrian magmatism at SW Iberian section of the African-Gondwana margin: Geochemical and isotopic keys to an incipient tectonic switching

Rojo-Pérez, Esther[1*]; Arenas, Ricardo[1]; Fuenlabrada, José M.[2]; Novo-Fernández, Irene[1]; Sánchez Martínez, Sonia[1]; Moreno-Martín, Diana[1]; Díez Fernández, Rubén[3]

[1]Departamento de Mineralogía y Petrología and Instituto de Geociencias (UCM, CSIC), Universidad Complutense. 28040 Madrid, Spain.

[2]Unidad de Geocronología (CAI de Ciencias de la Tierra y Arqueometría), Universidad Complutense. 28040 Madrid, Spain.

[3]Centro Nacional Instituto Geológico y Minero de España, CSIC, 37001 Salamanca, Spain.

*Corresponding author at: Departamento de Mineralogía y Petrología e Instituto de Geociencias (UCM, CSIC), Facultad de Geología, Universidad Complutense de Madrid. C/ José Antonio Novais, nª 12, 28040 Madrid, Spain. Tel.: +34 913944904

E-mail addresses:

e.rojo@ucm.es (Esther Rojo-Pérez) ORCID ID: 0000-0001-5780-6417

rarenas@ucm.es (Ricardo. Arenas)

jmfuenla@ucm.es (José Manuel Fuenlabrada)

inovo@ucm.es (Irene Novo-Fernández)

s.sanchez@ucm.es (Sonia Sánchez Martínez)

diamor03@ucm.es (Diana Moreno-Martín)

r.diez@igme.es (Rubén Díez Fernández)

Abstract

Pieces of the Pan-African-Cadomian arc evolution have been recognized through some European massifs. The Ossa-Morena Complex (SW Iberian Massif) is one of the best-preserved sections of this paleo-Gondwana margin. In this domain, recent studies consider that the magmatism related to the arc followed a cyclical pattern during the Late Ediacaran and Early Cambrian. However, its initial and more mature stages remain unclear.

Late Ediacaran magmatism (c. 602 Ma) in this section appears to be uninterrupted and driven by slab-mantle wedge-upper plate interactions. Early Paleozoic was a moment of significant changes along the Gondwana margin. In the Ossa-Morena Complex the beginning of the Cambrian (c. 541 Ma) appears marked by a deep unconformity over the Ediacaran basement, which is linked with the destabilization of the arc. However, the subduction-related magmatism continued with an increasing regularly mantle volume input driving to a more alkalinity geochemistry. This manuscript completes the geochemical and isotopic research of the peri-Gondwana arc evolution preserved in the SW Iberia during this period. These results point out shifts on geochemistry related to a higher slab angle in each magmatic cycle. It is possible to suggest a tectonic switching toward an extensional dynamic in this section of the Gondwana margin.

Keywords: North-African Gondwana margin, Ediacaran-Cambrian arc, tectonic switching, Cambrian magmatism.

Introduction

The orogenic belts where the oceanic lithosphere subducts under the continental lithosphere generates important volumes of igneous rocks associated with volcanic arcs. Orogens such as the Andean, are characterized by the generation of a large volume of intermediate-felsic rocks with minor amounts of mafic material. However, every magmatic event in the arc-cycle displays different geochemical features which allow to trace its geodynamic evolution. The eventual collision and cortical stacking related to the opening and closure of basins in active margin settings generate crustal thickening accompanied by margin and/or arc reworking and recycling. In these environments, crustal recycling plays a key role (e.g., Martin et al. 2005; Condie et al. 2011; Stern, 2020; Castro et al. 2021). An increasing number of studies have recognized the episodic nature of the magmatism in arcs (e.g., Mitchell et al. 2019; Li et al. 2019; Arenas et al. 2021). This cyclical nature and the geochemical features of the magmatic events are controlled internally by the tectonics of the subduction zone, which reflects the interaction between the slab and the upper plate input, as well as fluctuations generated in the mantle wedge (e.g., Jarrard, 1986; Archibald and Murphy, 2020). These factors determine the contribution of mantle-crust-slab material to the resulting melt. Traditionally, field descriptions accompanied by petrographic and major and trace elements features were the tools used to understand the tectonic setting and compositional evolution of arc-generated rocks. (e.g., Brown et al. 1984; Davidson, 1996; Andonaegui et al. 2016; El Haïbi et al. 2021). However, this evolution may remain partially obscured in ancient (largely dismanteled) arcs by subsequent metamorphic and deformational events. In these cases, the additional use of isotopic and geochronological tools is even more essential to constrain its origin and evolution.

The pre-Variscan basement preserved in European (Fig. 1) and North African massifs records at least one geodynamic cycle spanning from the Late Proterozoic to the Early Paleozoic, traditionally referred to as the Pan-African-Cadomian Orogeny (e.g., Murphy et al. 2002; Nance et al. 2002; Errami et al. 2009; Linnenamnn et al. 2014; von Raumer et al. 2015; Díez Fernández et al. 2019; Arenas et al. submitted). During this period, significant tectonic shifts were experienced on the Gondwana margin, such as the opening and closure of basins, derived from the variation of subduction-related parameters and processes beneath this margin (Chantraine et al. 2001; Kounov et al. 2012; Díez Fernández et al. 2019; Moradi et al. 2022; Arenas et al. submitted) These variations affected the dynamics of arc magmatism, including periodicity and geochemical composition of the successive magmatic episodes as determined by slab-mantle-upper plate interactions.

The activity in the Gondwana margin section located north of the Northwest African Craton spanned ca. 250 Ma (e.g., Albert et al. 2015). Although not all sectors preserving the pre-Paleozoic basement have recorded its whole evolution. The geochronological record extracted from detrital zircons of Late Proterozoic metasedimentary series and igneous rocks suggests an age of c. 750-730 Ma for the onset of subduction-associated magmatic activity in this section (e.g., Ordoñez-Casado, 1998; El Hadi et al. 2010; Pereira, 2015; Albert et al. 2015; Rojo-Pérez et al. 2022 and references therein). The magmatic activity of this arc system is estimated to have extended even into part of the Cambrian. However, the earliest and the mature stages remain poorly understood and do not appear uniformly preserved along the margin.

In the SW Iberian Massif, the most mature/evolved magmatic pulses are thought to be of the Andean-type (c. 541-534 Ma; Quesada, 1990; Sarrionandia et al. 2012; 2020). This type of magmatism suggests that subduction beneath the North African Gondwana margin remained active until at least the Early Cambrian and likely related with extension in the upper plate (e.g., Chichorro et al. 2008; Sánchez-García et al. 2010; Andonaegui et al. 2012; Albert et al. 2015; Díez Fernández et al. 2015; 2019). Although an extensional setting seems to dominate in this section of the Gondwana margin at the end of the Cambrian, the causes and timing of subduction cessation and/or tectonic switching remain poorly understood.

Geological setting

The Ossa-Morena Complex (OMC, SW Iberian Massif; Fig. 2a) represents a part of the Upper Allochthonous Terranes with continuation in NW Iberia (Díez Fernández and Arenas, 2015), defining the outermost section of the Pan-African margin of Gondwana. There is consensus that pre-Variscan deformation in Late Ediacaran and Early Cambrian rocks was related to subduction dynamics beneath this margin for an extended period (e.g., Quesada, 1990; Eguíluz et al. 2000; Linnemann et al. 2014; Díez Fernández et al. 2019; 2022; Arenas et al. submitted). The arc system was built on a thinned and extended section of the Gondwana margin, as indicated by the isotopic signature of the preserved metasedimentary sequences (López-Guijarro, 2006; López-Guijarro et al. 2008; Rojo-Pérez et al. 2019; 2021).

The Neoproterozoic sedimentary basement of the OMC has been traditionally referred to as the Serie Negra Group (Carvalhosa, 1965). This series has been classically divided in two different sequences, the Montemolín and Tentudía formations, whose boundary is poorly defined. The Montemolín Formation is formed by immature metasedimentary rocks (shales, slates and metagreywackes, essentially) and constitute the older and lower part of this series. The metasediments interbed with metabasites (metadolerites) layers of variable thickness, whose formation has been interpreted in relation to a suprasubduction setting (e.g., Ordóñez-Casado, 1998; Eguíluz et al. 1990; Sánchez-Lorda et al. 2016; Arenas et al. 2018; Rojo-Pérez et al. 2022). These rocks constitute the oldest recorded episode of arc construction, providing an age to the Montemolín Fm. close to c. 600 Ma (Ordoñez-Casado, 1998). Towards higher levels, the Tentudía Formation contains especially volcanogenic metagreywackes, metasandstones, slates and phyllites, black quartzites, metacherts and layers of micaschists and limestones. The maximum sedimentation age attributed to this formation has been classically established into a wide range between c. 565-541 Ma (U-Pb detrital zircons; Schäfer et al. 1993; Linnemann et al. 2008; Pereira, 2015). The whole-rock geochemistry and Nd-Sr isotopic sources of the Serie Negra are consistent with a convergence scenario relating to a continental arc built on a thinned crust (e.g., Bandrés, 2001; Bandrés et al. 2004; Rojo Pérez et al. 2019; 2021). This scenario is shared with intrusive granitic bodies, whose generation has been linked in part to slab melting and mantle wedge (Rojo-Pérez et al. 2022).

Overlying the Serie Negra Group and crossing the Ediacaran-Cambrian boundary, the Malcocinado Formation rests discordantly (Fig. 2b). This formation was originally described by Fricke (1941) and completed by Delgado-Quesada (1971) and Liñán (1978). This metavolcanoclastic succession contains andesitic metabreccias, massive metaandesites, metarhyolites and metadacites, metacinerites, phyllites, metasandstones, polygenic metaconglomerates and metacarbonates. In the northern OMC (Obejo-Valsequillo Domain), the Malcocinado Fm. crops out as patches (e.g., Apalategui et al. 1988; Martínez Poyatos, 1998; Bandrés and Eguíluz, 1999), while in the southern OMC, this formation has been observed at both sides of the Olivenza-Monesterio Antiform, Usagre and Llerena-Zafra (Fricke, 1941; Apalategui et al. 1984; 1985; Sánchez Carretero et al. 1989; Carracedo-Sánchez et al. 2007). This formation is also intruded by metagranitic bodies which complete the main magmatic record of the Pan-African-Cadomian cycle (e.g., La Bomba, Ahillones and El Escribano: Sánchez Carretero et al. 1989, 1990; Bandrés, 2001; Eguíluz et al. 2013), although these remain poorly studied.

The first U-Pb dates on zircons of this formation were obtained by Ordóñez-Casado (1998), who determined an age of c. 522 Ma for a reworked tuff and c. 514 Ma for a porphyritic rhyolite. A slightly older minimum sedimentation age c. 534 ±4 Ma (U-Pb, laser ablation in zircons) has been described recently by Sarrionandia et al. (2020) in a massive andesite. This age is nearly synchronous with the age suggested for the obduction of the Calzadilla Ophiolite (ca. 539 ±13 Ma, Arenas et al. 2018; Díez Fernández et al. 2019), which is related to the late stages of the arc-cycle.

Malcocinado Formation reference section

Volcanic and volcanoclastic rocks represent the main parts of the Malcocinado Formation. Above mafic and ultramafic rocks comprising the Calzadilla Ophiolite (Aguayo Fernández, 1985; Arenas et al. 2018), the bottom of the Malcocinado Formation rests discordant. This lower part is composed by conglomerates of variable thickness, with weak deformation and low-grade metamorphism, however it does not appear in all sectors where have been described analogous sequences. Polygenic conglomerates with volcano-sedimentary matrix re-appear at the top of the formation (Delgado-Quesada, 1971; Pérez-Lorente, 1979). The reworked material increases upwards, being arkosic at the transition to the Cambrian overlying unit (the Torreárboles Formation; Eguíluz et al. 2000).

A section of the Malcocinado Formation crops out exceptionally well near the village from which its name is derived. This section of volcano-sedimentary origin has an approximate thickness of c. 2000 m and includes mostly calc-alkaline volcanic lithologies intruded by at least one plutonic body. The reference schematic column of the Malcocinado Formation may be followed in Figure 2b. The bottom of the formation is not exposed in this section. The materials found ascending in the sequence are the following. 1) Andesitic-dacitic metabreccias. These rocks are formed by angular fragments of porphyritic andesites and dacites surrounded by a matrix with the same composition (Fig. 3a). The fracturing shown by these rocks suggests an important thermal contrast during its generation. The cooled edges shown by some of the included fragments (hyaloclastites, glassy tuffs, crystalline tuffs) are also indicative of this contrast (Fig. 3b). This suite of breccias is the thickest level into the sequence. 2) Discrete, thin levels of fine-grained sedimentary rocks. 3) Massive levels of metaandesites, metadacites, and metarhyolites (Fig. 3c), where the samples for analysis were collected. There are also some massive fine-grained levels, which may correspond to cinerite layers. Towards the top of the formation, the fragments included in the breccias vary in size and nature, appearing at some points massive aphanitic materials that may be derived from volcanic glass, including some flame structures (Fig. 3d). These rock fragments are generally poorly deformed, although deformation is heterogeneous through the sequence. The series is intruded by a granitic-granodioritic massif, which is considered coeval with this formation. 4) The materials located in the upper part of the Malcocinado Formation are essentially clastic-supported metaconglomerates, with volcanoclastic matrix (Fig. 3e and 3f). The pebbles correspond to reworked immature metasediments and acidic-intermediate volcanic rocks. Some of them are variably sized structured rocks floating dispersed in a matrix cemented by pyroclastic material. The rounding of these pebbles indicates high-energy transport in a possibly aqueous medium (Fig. 3e and 3f) and suggesting strong erosion of all previous arc materials. The amount of reworked material increases upwards the formation.

Sample selection and methodology

Sample selection

Fourteen samples of metaigneous rocks were selected for whole-rock and isotopic (Sr-Nd) analysis. All samples were collected from outcrops at the reference section (Fig. 2a). . Sampling was focused on collecting the most representative and unaltered samples, avoiding the sections affected by late fracturing and fluid percolation. Sample locations are included in Table 1. Two groups of samples have been differentiated in this formation. Ten samples of massive metavolcanic rocks. Within this group, andesites are the most abundant lithologies, although dacites and a felsic volcanic rock were also sampled. The remaining four samples belong to the intrusive metagranitic massif

Whole-rock major and trace elements analysis

Samples were crushed and pulverized for the analyses at the Universidad Complutense de Madrid. Major and trace elements analyses were performed at Activation Laboratories (ActLabs), Ontario (Canada). Sample fusion was performed with lithium metaborate/tetraborate. Major and some trace elements were determined by ICP-OES, while most trace elements were measured by ICP-MS. The detection limits of the analytical procedure range from 0.01% for most major elements to 0.001% for TiO2 and MnO. Results of major and trace element analyses are included in Table 2 and the main compositional features are shown in figures included in Results section (Figs. 5 to 7).

Whole-rock Sr-Nd isotopic analysis

Sr-Nd isotopic analyses were performed at the Geochronology Unit (CAI of Earth Sciences and Archaeometry; https://cai.ucm.es/ciencias-tierra-arqueometria/geocronologia/) of the Universidad Complutense de Madrid, by TIMS (Thermal Ionization Mass Spectrometry). The samples were dissolved with ultrapure reagents (HF, HNO_3, HCl) in successive heating and evaporation steps. In a first chromatographic separation step (using Resin Dowex AG®50x8) the Sr (free of Rb) and REE fractions were extracted from the matrix; while in a second step, Nd was separated from Sm using an extraction resin (Ln-Resin®). Sr and Nd samples were analyzed in an IsotopX-Phoenix® mass spectrometer (TIMS), following a dynamic multicollection model. Potential ^{87}Rb

interferences were corrected for $^{87}Sr/^{86}Sr$ ratios and normalized to the average $^{86}Sr/^{88}Sr$ value of 0.1194 (Nier, 1938), used for conventional inner corrections. The final Sr isotope ratios were corrected by considering the Sr standard isotope ratios (NBS 987 - Standard Reference Material 987), analyzed together with the samples and providing an average value of $^{87}Sr/^{86}Sr$ = 0.710246 (±0.000017; 2σ) for 10 standard replicates. In order to correct for procedural and instrumental mass fractionation, the $^{143}Nd/^{144}Nd$ ratios were normalized to the value of $^{146}Nd/^{144}Nd$ = 07219 (O'Nions et al. 1979) and corrected for potential interferences from ^{142}Ce and ^{144}Sm. Deviations from the isotopic ratios of the samples were corrected using the Nd isotopic standard values (JNdi-1; Tanaka et al. 2000). Analysis of 7 replicate of this standard together with the samples provided an average value of $^{143}Nd/^{144}Nd$= 0.512112 with an internal precision of ±0.000009 (2σ). Analytical biases in the $^{87}Sr/^{86}Sr$ and $^{143}Nd/^{144}Nd$ ratios were estimated to be lower than 0.01% and 0.006%, respectively. The Sr and Nd blank are always under 0.5 and 0.1 ng, respectively. The results of the Sr and Nd isotopic analyses are summarized in Table 3 and the main isotopic features are plotted in the diagrams included in Fig. 8 into the Results section.

Results

Petrographic features

Thin sections were prepared of all the selected samples. Under microscope, the primary minerals of the volcanic rocks appear to be completely replaced by other low temperature secondary minerals. Matrix of the metaandesites and metadacites is mostly chlorite and opaque minerals, although these still preserve plagioclase pseudomorphs (Figs. 4a and 4b). Sarrionandia et al. (2020) suggest the existence of extensive albitisation and chloritization processes in these rocks, as a product of interaction with seawater at low temperature. In thin section, the metagranites show close to eutectic mineral assemblage. Intergrowth textures are abundant (Figs. 4c and 4d), indicative of shallow emplacement. Plagioclase usually preserves in many cases primary igneous idiomorphic texture, although it is mostly saussuritized. The few mafic preserved minerals are biotite, mostly replaced by chlorite.

Whole rock geochemistry

Metaandesites show slightly higher Fe_2O_3, MgO, CaO, and Na_2O contents, while metadacites and metarhyolites show higher SiO_2 and K_2O contents. The average TiO_2, Al_2O_3, MnO, and P_2O_5 contents are similar in all metavolcanic samples (Table 2). In plutonic rocks, major elements are uniform in all samples (Table 2), and similar to the metadacites-rhyolites in the contents of TiO_2, Fe_2O_3, MgO, K_2O, and P_2O_5, with slightly higher MnO contents. While CaO and Na_2O contents are closer to the metaandesites values.

Considering the high LOI value (in some cases >2-3 wt%), the rocks were classified according to the Nb/Y-Zr/Ti diagram (Winchester and Floyd, 1977, modified by Pearce, 1996a; Fig. 5a). Six samples appear represented in the field of andesites and basaltic andesites, three samples show dacitic composition and one has rhyolitic nature. The rocks studied follow a potassium-rich calc-alkaline trend, transiting to shoshonitic, according to the Co/Th diagram (Hastie et al. 2007; Fig. 5b). On the other hand, plutonic rocks are metagranodiorites at the Nb/Y-Zr/Ti diagram (Fig. 5a). All of them are ferroan granites in relation to their nFe, occurring mostly in the alkaline-calcic field on the MALI diagram (Figs. 5c and 5d; Frost et al. 2001; Frost and Fost, 2011). These bodies are also essentially peraluminous (Shand, 1943) and show compositions close to those of the Cordilleran batholiths (Frost et al. 2001).

Chondrite normalized REE (Sun and McDonough, 1989) exhibit two distinct trends. Andesites show weakly fractionated patterns, with slightly enriched LREE ($(La/Sm)_N$=1.84-3.05) and almost flat HREE patterns ($(Gd/Yb)_N$=1.04-1.57). These rocks show a slight negative Eu anomaly (Eu/Eu* = 0.22-0.30) and a positive Dy anomaly (Fig. 6a). Intermediate-felsic rocks (metagranites, metadacites and metarhyolite) display more fractionated patterns, with significant LREE enrichment ($(La/Sm)_N$=3.40-5.39) and slightly more enriched HREE patterns ($(Gd/Yb)_N$=0.92-1.94). These rocks show a significant negative Eu anomaly (Eu/Eu* = 0.16-0.22) and positive Dy anomaly (Fig. 6b).

Primitive Mantle normalized trace elements (McDonough and Sun 1995) also depict two groups of patterns. Metaandesite show enriched LILE, with variable contents in most of the mobile elements (Cs, Rb, Ba, K) and HFSE patterns close to the unit (Fig. 6c). These rocks display negative Nb and Ti anomaly, along with positive anomalies in Pb and K. Metadacites-metarhyolites and metagranodiorites show more homogeneous trace element patterns with higher fractionation between LILE and HFSE (Fig. 6d). These rocks exhibit reduced mobility in lighter elements, with significant negative anomalies in Nb, Sr, P, and Ti, and slightly positive in Th, U, and Pb.

Massive andesites with adakitic signatures have been described in other sectors of the Ossa-Morena Complex within this formation (Sarrionandia et al. 2020). Nevertheless, according to the Yb_N vs. $(La/Yb)_N$ diagram (Martin, 1986; MacPherson et al. 2006; Fig. 7a), the studied metaandesites show geochemical patterns associated with common volcanic-arc rocks (Defant and Drummond, 1990; Drummond et al. 1996; Martin et al. 2005; MacPherson et al. 2006), away from the adakitic rocks field. These rocks have high Th/Yb contents, appearing displaced from the MORB-OIB array towards an arc supra-subduction setting on the Th/Yb-Nb/Yb diagram (Fig. 7b; Pearce, 1982, 2008).

An arc-linked tectonic setting is also compatible with the genesis of the metagranites intruding the Malcocinado Fm. (Pearce et al. 1984; Pearce, 1996b). The studied samples are represented in the VAG field, within the area representing modern Chile-type arcs (Fig. 7c; Pearce, 1996b). The Rb, Y+Nb, and Ta+Yb contents are similar in all samples and tend towards slightly more alkaline values, close to intraplate granites. According to the tectono-magmatic Th-Hf-Nb diagram (Fig. 7d; Wood, 1980), employed to unify the above observations, all studied metaigneous rocks share calc-alkaline signature, suggesting a common subduction scenario for the magma source.

Sr-Nd isotopic geochemistry

The latest published age of the Malcocinado Formation (c. 534 Ma; Sarrionandia et al. 2020) was taken for Nd and Sr calculations of metavolcanites (Table 3). Based on the intrusive relationship between these rocks and the metagranitic bodies, the same age was considered as reference for the Nd and Sr calculations of the studied metagranodiorites. The metaigneous rocks of the Malcocinado Formation show negative $\varepsilon Nd_{(0)}$ values. The metavolcanites exhibit heterogeneous values (between -0.2 and -8.6), while the metagranodiorites describe more restricted values (between -4.0 and -5.5; Figs. 8a and 8b). The $\varepsilon Nd_{(t)}$ values show large variation in the metavolcanites, from strongly negative values close to those established for continental crust-derived rocks (eg., DePaolo and Wasserburg, 1976; White, 2015), to positive values (Figs. 8a and 8b). The metagranodiorite samples exhibit less variation in $\varepsilon Nd_{(t)}$ values (between 0.6 and 2.5; Figs. 8a and 8b; Table 3). The model ages of the studied metaigneous rocks conforming the Malcocinado Formation (Fig. 8a; calculated according to DePaolo, 1988) ranging from T_{DM}=841-1410 Ma. The most homogeneous model ages are provided by the metagranodiorites, ranging from 841 to 988 Ma, falling entirely within the range defined by the Mérida metagranitic complexes. While the metavolcanites show a wider range of values, between 883 and 1410 Ma, heterogeneously distributed and slightly overlapping the range calculated for the metabasites of the Montemolín Formation(Fig. 8a; Rojo-Pérez et al. 2022). Sr values show restrictive values on metagranodiorites, while the metavolcanic rocks display large variation (Fig. 8b).

Discussion and conclusions

Most accretionary orogens typically preserve evidence of recurring extension and contraction events or stages, which leading the opening and closure of basins on active margins. Furthermore, extensional stages may occur almost synchronously with collisional stages, even in adjoining regions of the same margin (e.g., Collins, 2002a and b; Cawood et al. 2009). In addition, these events have been eventually associated with arc migration towards the trench (Glen, 2005; Collins and Richards, 2008; Collins et al. 2020), and changes in magmatism. Cyclicity in active margin magmatism operating on active margins is influenced by slab-mantle-upper plate interactions. Initial stages and contractional events seem to correlate with a lower subduction angle and a greater input of crustal material to the subduction channel (Bourgois et al. 1996; Kay, 1978; Kay et al. 2005). While greater subduction angles are related to episodes of slab roll-back and extension in the upper plate (e.g., Collins, 2002b; Collins et al. 2020, Díez Fernández et al. 2015; 2019). In long-lived arc margins, this cyclicity eventually tends towards higher slab angles in each episode, whose imprint on magmatism is visible through the geochemistry and isotopic sources of the generated melts (Collins, 2002b; Collins et al. 2020). In some Pan-African-Cadomian Orogen domains, discrete contraction to extension events have been described usually attributed to some type of collision, followed by extension/rifting stages (e.g., Gasquet et al. 2005; Errami et al. 2009; Nouri et al. 2022 and references therein). In western sectors, close to the West African Craton, this cyclicity is also reported during the Ediacaran times (Arenas et al. 2018, submitted; Díez Fernández et al. 2022; Rojo-Pérez et al. 2022). Although the latest subduction-related magmatism stages, at the beginning of Cambrian times, remain unclear in this section of the Gondwana margin.

Geochemistry and isotopic sources during Ediacaran-Cambrian transition

The Ossa-Morena Complex contains a well-preserved representation of Cadomian-Avalonian continental arc magmatism, the cyclical magmatic events recorded in the Mérida Massif (N of the OMC) range from c. pre-602 to 541 Ma (Rojo Pérez et al. 2022). The most mature stage of the Cadomian-Avalonian arc has been traditionally represented by the Malcocinado Formation in this section of the Gondwanan margin.

The Malcocinado Fm. metavolcanites exhibit a strong subduction-related signature, as typified by their calc-alkaline nature with tendency towards higher K contents (Fig. 5b), and the significant negative Nb and Ti anomalies, and the relative Th enrichment (Fig. 6a). The arc-related setting is also supported by the high Th/Y values of metaandesites regarding the MORB-OIB array (Fig. 7b), which suggests a genesis from a mantle source influenced by fluid input and/or partial melting of material extracted from the slab. This geochemical signature has been also described in the oldest (Montemolín Formation) mafic magmatism preserved in this margin section, follow by magmatic episodes with adakitic signature (Rojo-Pérez et al. 2022). At the mature stage of this arc, Sarrionandia et al. (2020) describe again adakite nature for the metaandesites of the Malcocinado Formation. However, according to the geochemistry of analyzed rocks from the Malcocinado Formation, the existence of adakitic-signature materials cannot be confirmed in the studied region (Fig. 7a). The wide range in the $\varepsilon Nd_{(t)}$ (-3.5 to 3.0) and T_{DM} values (883 to 1410 Ma; Fig. 8a) is far away from of the apparent model ages that depleted mantle-derived rocks should have at 534 Ma. However, these differences in isotopic parameters are not exclusive of these rocks and have been recently described in the metabasites of Montemolín Fm. (Rojo-Pérez et al. 2022), being consistent with an derivation from a largely modified mantle wedge.

Fractional crystallization evolution from an enriched mantle was also suggested for latest stages of the peri-Gondwanan arc construction (c. 541 Ma; Rojo-Pérez et al. 2022), displaying a typical Cordilleran granites signature. The next pulse, studied in this research, exhibits rather a calc-alkaline to alkaline-calcic and ferroan behaviour (Fig. 5c and 5d). Although, most of ferroan granites belong to the so-called A-type granites (Frost and Frost, 2011), in subduction settings such granites may be generated by abundant partial melting of calc-alkaline magnesian granitoids under low-pressure conditions (Eby, 1992; Skjerlie and Johnston, 1993; Frost and Frost, 2011; and references therein). The intergrowth textures (graphics) typical of melts crystallized at shallow crust shown by these rocks support a low-pressure conditions.

Compared to the Ediacaran pulses of the continental arc, an increasing input from the mantle during the Early Cambrian is suggested by positive εNd along with model ages (TDM) closer to protolith crystallization ages and to those calculated for the previous (Ediacaran) roll-back magmatic episode (Fig. 8a; Rojo-Pérez et al. 2022). This is also supported by the mantle signature of Sr isotopes, which plot close to the Mérida metagranitic complexes (Fig.8b). Although departing slightly from the traditional chemistry expected for Cordilleran granites, Nd and Sr isotopic sources of the Malcocinado Formation plot close to the calculated paths for Andean batholiths (Fig. 8b; Castro et al. 2021). The cyclicity of Ediacaran-Cambrian magmatism (Rojo-Pérez et al. 2022) seems also in agreement with recent modeling, proposing an alternation of felsic and intermediate-basic magmatic episodes (e.g., Collins et al. 2020). Considering the geochemistry of studied metaigneous rocks, mature stages of the arc in this section would transit to a more alkaline magmatism, with a higher input of mantle material in each cycle.

Tectonic setting: an incipient geodynamic switching

These changes in magmatism have been linked to progressively higher subduction angles. In these dynamic conditions the upper plate extensional and compressional events generate the opening and closure of basins (Arenas et al. 2018, Submitted; Díez Fernández et al. 2019; 2022). A well-recorded geodynamic event of this Cadomian cycle with contractional character appear preserved along the Variscan Belt at c. 550-540 Ma (e.g., Quesada, 1990; Eguíluz et al. 2000; Bandrés et al. 2004; Rojo-Pérez et al. 2022; Arenas et al. submitted). In the OMC, this event has recently been related to the closure, accretion and obduction of oceanic domains (Arenas et al. 2018), coeval with arc-continent collision and accretion of the external Gondwana margin under the volcanic arc (Díez Fernández et al. 2022; Arenas et al. submitted). This compressional stage is almost synchronous with the last Late Ediacaran magmatic episode of the arc construction dated at c. 541 Ma, which has been linked to roll-back dynamics and a lower input of cortical material into the subduction zone (Rojo-Pérez et al. 2022). The virtually equivalent age of this pulse and the sedimentation of the oldest part of the Malcocinado Fm. is compatible with the destabilization and erosion of the arc towards the end of Ediacaran times, generating the unconformity on which it was deposited (Fig. 9). The overlapping of magmatic cycles separated by destabilization and erosion stages seen in this section of the Gondwanan margin, is common in different volcanic arc systems (e.g., Stern, 1994; Meert, 2003; Fritzet al. 2013). Analogous unconformities at the same period of age have been reported and interpreted as evidence of tectonic switching across peri-Gondwana (e.g., Ma et al. 2022).

Although magmatism of this formation still exhibits a continental arc signature, its slightly more alkaline signature has been also associated with post-collisional magmatism in subduction settings(Figs. 7c and 9; Pearce et al. 1984; Eby, 1992). This would agree with its generation after an accretionary and compressional stage recorded on this margin (e.g., Quesada, 1990; Díez Fernández et al. 2022; Arenas et al. submitted). An increasing angle of subduction would explain the geochemical and isotopic characteristics shown by the magmatism in early Cambrian times in this section of the Gondwana margin. It would limit the input of tectonic erosion and on the other hand, it would increase the volume of mantle input in the resulting melt. In the modelling of Andean-type orogens, the presence of thick mantle wedges formed during and after prolonged subduction together with slab roll-back has been suggested may contribute to upper plate extension (Fig. 9; e.g., Rey and Müller, 2010; Gómez-Tuena et al. 2014; Díez Fernández et al. 2015; Parolari et al. 2021).

These data suggest the beginning of a deep geodynamic switching on the Gondwana margin, compatible with the transition towards an increasingly extensional regime (e.g., Díez Fernández et al. 2015; 2019; 2022). In these dynamic settings, the prolonged attenuation of the lithosphere commonly leads to the eventual basins formation and the sedimentation of mostly clastic and/or carbonate deposits, possibly analogous to the materials that appear culminating in the Malcocinado Formation and start the overlying Cambrian formation (Liñan, 1984).

Acknowledgements

Financial support has been provided by Spanish projects CGL2016-76438-P, PID2020-112489GB-C21 and PID2020-112489GB-C22 funded by MCIN/AEI/ 10.13039/501100011033, and the associated grant BES-2017-080200.

References

Aguayo Fernández, J.M. 1985. Rocas ultramáficas en el sector de Calzadilla de los Barros (Badajoz). [Master Thesis]. Universidad del País Vasco, 110 p.

Albert, R., Arenas, R., Gerdes, A., Sánchez Martínez, S., Fernández-Suárez, J. and Fuenlabrada, J.M. 2015. Provenance of the Variscan Upper Allochthon (Cabo Ortegal Complex, NW Iberian Massif). Gondwana Research, 28, 1434–1448.

Andonaegui, P., Castiñeiras, P., González Cuadra, P., Arenas, R., Sánchez Martínez, S., Abati, J., Díaz García, F. and Martínez Catalán, J.R. 2012. The Corredoiras orthogneiss (NW Iberian Massif): geochemistry and geochronology of the Paleozoic magmatic suite developed in a peri-Gondwanan arc. Lithos 128-131, 84–99.

Andonaegui, P., Arenas, R., Albert, R., Sánchez Martínez, S., Díez Fernández, R. and Gerdes, A. 2016. The last stages of the Avalonian-Cadomian arc in NW Iberian Massif: isotopic and igneous record for a long-lived peri-Gondwanan magmatic arc. Tectonophysics, 681, 06–14.

Apalategui, O., Garrote, A., Higueras, P., Odriozola, J.M. and Peon, A. 1984. Mapa y memoria explicativa de la Hoja 1: 50.000, Nº. 877 (L1erena) del Mapa geológico Nacional (MAGNA). Instituto Geológico y Minero de España (IGME), Madrid.

Apalategui, O., Borrero, J., Delgado Quesada, M., Roldan, F.J., Garrote. A. and Eguiluz, L. 1985. Mapa y memoria explicativa de la Hoja 1: 50.000, Nº. 899 (Guadalcanal) del Mapa geológico Nacional (MAGNA). Instituto Geológico y Minero de España (IGME), Madrid.

Apalategui, O., Contreras, F., Jorquera, A., Villalobos, M. and Eguíluz, L. 1988. Mapa y memoria explicativa de la Hoja 1:50.000, Nº 804 (Oliva de Mérida) del Mapa Geológico Nacional (MAGNA). Instituto Geológico y Minero de España (IGME), Madrid.

Archibald, D.B. and Murphy, J.B. 2021. A slab failure origin for the Donegal composite batholith, Ireland as indicated by trace-element geochemistry. Geological Society, London, Special Publications, 503, 347–370.

Arenas, R., Sánchez Martínez, S., Díez Fernández, R., Gerdes, A., Abati, J., Fernández-Suárez, J., Andonaegui, P., González Cuadra, P., López Carmona, A., Albert, R., Fuenlabrada, J.M. and Rubio Pascual, F.J. 2016.

Allochthonous terranes involved in the Variscan suture of NW Iberia: a review of their origin and tectonothermal evolution. Earth Sciences Reviews, 161, 140–178.

Arenas, R., Fernández-Suárez, J., Montero, P., Díez Fernández, R., Andonaegui, P., Sánchez Martínez, S., Albert, R., Fuenlabrada, J.M., Matas, J., Martín Parra, L.M., Rubio Pascual, F.J., Jiménez-Díaz, A. and Pereira, M.F. 2018. The Calzadilla Ophiolite (SW Iberia) and the Ediacaran fore-arc evolution of the African margin of Gondwana. Gondwana Research, 58, 71–86.

Arenas, R., Sánchez Martínez, S., Albert, R., Haissen, F., Fernández- Suárez, J., Pujol- Solà, N., Andonaegui, P., Díez Fernández, R., Proenza, J.A., García-Casco, A. and Gerdes, A. 2021. 100 myr cycles of oceanic lithosphere generation in peri- Gondwana: Neoproterozoic–Devonian ophiolites from the NW African–Iberian margin of Gondwana and the Variscan Orogen. In: Murphy, J.N., Strachan, R.A., Quesada, C. (Eds.), Pannotia to Pangaea: Neoproterozoic and Paleozoic Orogenic Cycles in the Circum-Atlantic Region. Geological Society, London, Special Publications, 503, 169-184.

Arenas, R., Rojo-Pérez, E., Díez Fernández, R; Albert, R., Novo-Fernández, I; Sánchez Martínez, S., Fuenlabrada, J.M., Andonaegui, P., Moreno-Martín, D., Gerdes, A. and García-Casco, A. Submitted. Opening and closure of Cadomian peri-Gondwanan oceans: age and evolution of the Mérida Ophiolite (SW Iberia). International Geology Review.

Bandrés, A. 2001. Evolución geodinámica poliorogénica de los dominios septentrionales de la ZOM. Phd tesis, Universidad del País Vasco, España, 377 p.

Bandrés, A. and Eguíluz, L. 1999. Litoestratigrafía de la formación El Hoyo (zona de Ossa-Morena, Macizo Ibérico, España). Geogaceta, 26, 3-6.

Bandrés, A., Eguíluz, L., Pin, C., Paquette, J.L., Ordóñez, B., Le Fèvre, B., Ortega, L.A. and Gil Ibarguchi, J.I. 2004. The northern Ossa-Morena Cadomian batholith (Iberian Massif): Magmatic arc origin and early evolution. International Journal of Earth Sciences, 93, 860–885.

Brown, G.C., Thorpe, R.S. and Webb, P.C. 1984. The geochemical chacteristics of granitoids in contrasting arcs and comments on magma sources. Journal of the Geological Society of London, 141, 413–426.

Bourgois, J., Martin, H., Lagabrielle, Y., Le Moigne, J. and Frutos Jara, J. 1996. Subduction erosion related to spreading-ridge subduction: Taitao peninsula (Chile margin triple junction area). Geology, 24, 723-726.

Carracedo-Sánchez, M., Sarrionaindía, F. and Gil Ibarguchi, J.I. 2007. Informe Sobre La petrogénesis, geoquímica y geocronología de La Formación Malcocinado en El Sector de Bienvenida-Usagre (Hojas de Usagre, Llerena Y Zafra). Zona de Ossa-Morena, Provincia de Badajoz. Open-File Report, IGME, 109 pp.

Carvalhosa, A. 1965. Contribuição para o conhecimento geológico da região entre Portel e Ficalho (Alentejo). Memorias dos Serviços Geológicos de Portugal, 11, 1-130.

Castro, A., Rodriguez, C., Fernández, C., Aragón, E., Pereira, M.F. and Molina, J.F. 2021. Secular variations of magma source compositions in the North Patagonian batholith from the Jurassic to Tertiary: Was mélange melting involved?. Geosphere, 17, 766–785.

Cawood, P.A., Kröner, A., Collins, W.J., Kusky, T.M., Mooney, W.D. and Windley, B.F. 2009. Accretionary orogens through Earth history. Geological Society, London, Special Publications, 318, 1-36.

Chantraine, J., Egal, E., Thiéblemont, D., Le Goff, E., Guerrot, C., Ballèvre, M., Guennoc, P. and 2001. The Cadomian active margin (North Armorican Massif, France): A segment of the North Atlantic Panafrican belt: Tectonophysics, 331, 1–18.

Chichorro, M., Pereira, M.F., Díaz-Azpiroz, M., Williams, I.S., Fernández, C., Pin, C. and Silva, J.B. 2008. Cambrian ensialic rift-related magmatism in the Ossa-Morena zone (Évora-Aracena metamorphic belt, SW Iberian Massif): Sm-Nd isotopes and SHRIMP zircon U-Th-Pb geochronology: Tectonophysics, 461, 91–113.

Collins, W.J. 2002a. Hot orogens, tectonic switching, and creation of continental crust. Geology, 30, 535-538.

Collins, W.J. 2002b. Nature of extensional accretionary orogens. Tectonics, 21, 1258–1272.

Collins, W.J. and Richards, S.W. 2008. Geodynamic significance of S-type granites in circum-Pacific orogens. Geology, 36, 559-562.

Collins, W.J., Huang, H.Q., Bowden, P. and Kemp, A.I.S. 2020. Repeated S–I–A-type granite trilogy in the Lachlan Orogen and geochemical contrasts with A-type granites in Nigeria: implications for petrogenesis and tectonic discrimination. Geological Society, London, Special Publications, 491, 53-76.

Condie, K.C., Bickford, M.E., Aster, R.C., Belousova, E. and Scholl, D.W. 2011. Episodic zircon ages, Hf isotopic composition, and the preservation rate of continental crust. Geological Society of America Bulletin, 123, 951–957.

Davidson, J.P. 1996, Deciphering mantle and crustal signatures in subduction zone magmatism: American Geophysical Union Geophysical Monograph, 96, 251–262.

Defant, M.J. and Drummond, M.S. 1990. Derivation of some modern arc magmas by melting of young subducted lithosphere. Nature, 347, 662–665.

Delgado-Quesada, M. 1971: Esquema geológico de la Hoja número 878 de Azuaga (Badajoz). Boletín Geológico y Minero, 82, 277-286.

DePaolo, D.J. 1981. A neodymiun and strontium isotopic study of the Mesozoic calcalkaline granitic batholiths of the Sierra-Nevada and Peninsular ranges, California. Journal of Geophysical Research, 86, 470–488.

DePaolo, D.J. 1988. Neodymium Isotope Geochemistry: An Introduction. Springer Verlag, New York.

DePaolo, D. and Wasserburg, G. 1976. Inferences about magma sources and mantle structure from variations of $^{143}Nd/^{144}Nd$. Geophysical Research Letters, 3, 743–746.

Díez Fernández, R. and Arenas, R. 2015. The Late Devonian Variscan suture of the Iberian Massif: A correlation of high-pressure belts in NW and SW Iberia. Tectonophysics, 654, 96–100.

Díez Fernández, R., Pereira, M.F. and Foster, D.A. 2015. Peralkaline and alkaline magmatism of the Ossa-Morena zone (SW Iberia): Age, source, and implications for the Paleozoic evolution of Gondwanan lithosphere. Lithosphere, 7, 73–90.

Díez Fernández, R., Jiménez-Díaz, A., Arenas, R., Pereira, M.F. and Fernández-Suárez, J. 2019. Ediacaran obduction of a fore-arc ophiolite in SW Iberia: a turning point in the evolving geodynamic setting of peri-Gondwana. Tectonics, 38, 95–119.

Díez Fernández, R., Arenas, R., Rojo-Pérez, E., Sánchez Martínez, S. and Fuenlabrada, J.M. 2022. Tectonostratigraphy of the Mérida Massif reveals a new Cadomian suture zone exposure in Gondwana (SW Iberia). International Geology Review, 64, 405-424.

Drummond, M.S., Defant, M.J. and Kepezhinskas, P.K. 1996. The petrogenesis of slab derived trondhjemite – tonalite – dacite / adakite magmas. Transactions of the Royal Society of Edinburgh: Earth Sciences, 87, 205–216.

Eby, G.N. 1992. Chemical subdivision of the A-type granitoids: Petrogenetic and tectonic implications. Geology, 20, 6416-44.

Eguíluz, L., Abalos, B. and Ortega Cuesta, L.A. 1990. Anfibolitas proterozoicas del sector central de la Zona de Ossa-Morena: geoquímica e implicaciones geodinámicas. Cadernos do Laboratorio Xeolóxico de Laxe, 15, 119–131.

Eguíluz, L, Gil Ibarbuchi, J.I., Ábalos, B. and Apraiz, A. 2000. Superposed Hercynian and Cadomian orogenic cycles in the Ossa-Morena zone and related areas of the Iberian Massif. Geological Society of America Bulletin, 112, 1398-1413.

Eguiluz, L., Iriondo, A. and Martínez-Torres, L.M. 2013. Edad 40Ar/39Ar (539, 06±3 Ma) de los anfíboles del Granitoide del Escribano: Arco volcánico cadomiense (zona de Ossa-Morena). Geogaceta, 54, 51-54.

El Hadi, H., Simancas, J.F., Martínez Poyatos, D., Azor, A., Tahiri, A., Montero, P., Fanning, C.M., Bea, F. and González-Lodeiro, F. 2010. Structural and geochronological constraints on the evolution of the Bou Azzer Neoproterozoic ophiolite (Anti-Atlas, Morocco). Precambrian Research, 182, 1–14.

El Haïbi, H., El Hadi, H., Pesquera, A., Tahiri, A., Martínez Poyatos, D., Zahour, G., Mehdioui, S. and Tahiri, M. 2021. Geochemical and Sr–Nd isotopic constraints on the petrogenesis of the Tiflet granitoids (Northwestern Moroccan Meseta): geological implications. Journal of Iberian Geology, 47, 347–365.

Errami, E., Bonin, B., Laduron, D. and Lasri, L. 2009. Petrology and geodynamic significance of the post-collisional Pan-African magmatism in the Eastern Saghro area (Anti-Atlas, Morocco). Journal of African Earth Sciences, 55, 105–124.

Franke, W. 1989. Tectonostratigraphic units in the Variscan belt of central Europe. In: Dallmeyer, R.D. (Ed.), Terranes in the Circum-Atlantic Paleozoic Orogens. Geological Society of America Special Papers, 230, 67-90.

Fricke, W. 1941. Die Geologie des Grenxebietes zwischen nordöstlicher Sierra Morena und Extremadura. PhD thesis, University of Berlin, Berlin, Germany, 91 pp.

Fritz, H., Abdelsalam, M., Ali, K.A., Bingen, B., Collins, A.S., Fowler, A.R., Ghebreab, W., Hauzenbergeer, C.A., Johnson, P.R., Kusky, T.M., Macey, P., Muhongo, S., Stern, R.J. and Viola, G. 2013. Orogen styles in the East African Orogen: a review of the Neoproterozoic to Cambrian tectonic evolution. Journal of African Earth Sciences, 86, 65-106.

Frost, C.D. and Frost, B.R. 2011. On ferroan (A-type) granitoids: their compositional variability and modes of origin. Journal of Petrology, 52, 39–53.

Frost, B.R., Barnes, C.G., Collins, W.J., Arculus, R.J., Ellis, D.J. and Frost, C.D. 2001. A geochemical classification for granitic rocks. Journal of Petrology, 42, 2033–2048.

Gasquet, D., Levresse, G., Cheilletz, A., Azizi-Samir, M.R. and Mouttaqi, A. 2005. Contribution to a geodynamic reconstruction of the Anti-Atlas (Morocco) during Pan-African times with the emphasis on inversion tectonics and metallogenic activity at the Precambrian–Cambrian transition. Precambrian Research, 140, 157–182.

Glen, R.A. 2005. The Tasmanides of eastern Australia. Geological Society, London, Special Publication, 246, 23–96.

Gómez-Tuena, A., Straub, S.M. and Zellmer, G.F. 2014. An introduction to orogenic andesites and crustal growth. Geological Society, London, Special Publications, 385, 1-13.

Hastie, A.R., Kerr, A.C., Pearce, J.A. and Mitchell, S.F. 2007. Classification of altered volcanic island rocks using immobile trace elements: development of the Th-Co discrimination diagram. Journal of Petrology, 48, 2341–2357.

Jacobsen, S.B. V Wasserburg, G.J. 1980. Sm-Nd isotopic evolution of chondrites. Earth and Planetary Science Letters, 50, 139–155.

Jarrard, R. D. 1986. Relations among subduction parameters. Reviews of Geophysics, 24, 217–284.

Kay, R.W. 1978. Aleutian magnesian andesites: melts from subducted Pacific Oceanic crust. Journal of Volcanology and Geothermal Research, 4, 117–132.

Kay, S.M., Godoy, E. and Kurtz, A. 2005. Episodic arcmigration, crustal thickening, subduction erosion, and magmatism in the south-central-Andes. Geological Society of America Bulletin, 117, 67–88.

Kounov, A., Graf, J., von Quadt, A., Bernoulli, D., Burg, J.P., Seward, D., Ivanov, Z. and Fanning, M. 2012. Evidence for a "Cadomian" ophiolite and magmatic-arc complex in SW Bulgaria. Precambrian Research, 212-213, 275–295.

Li, Z.X., Mitchell, R.N., Spencer, C.J., Ernst, R., Pisarevsky, S., Kirscher, U. and Murphy, J.B. 2019. Decoding Earth's rhythms: Modulation of supercontinent cycles by longer superocean episodes. Precambrian Research, 323, 1–5.

Linnemann, U., Pereira, M.F., Jeffries, T., Drost, K. and Gerdes, A. 2008. Cadomian Orogeny and the opening of the Rheic Ocean: new insights in the diachrony of geotectonic processes constrained by LA-ICP-MS U-Pb zircon dating (Ossa-Morena and Saxo-Thuringian Zones, Iberian and Bohemian Massifs). Tectonophysics, 461, 21–43.

Linnemann, U., Gerdes, A., Hofmann, M. and Marko, L. 2014. The Cadomian Orogen: Neoproterozoic to Early Cambrian crustal growth and orogenic zoning along the periphery of the West African Craton—constraints from U-Pb zircon ages and Hf isotopes (Schwarzburg Antiform, Germany). Precambrian Research, 244, 236–278.

Liñán, E. 1978. Bioestratigrafía de la Sierra de Córdoba. Phd tesis, Universidad de Granada, España, 212p.

Liñán, E. 1984. Los icnofósiles de la Formación Torreárboles (Precámbrico?–Cámbrico) en los alrededores de Fuente de Cantos, Badajoz. Cuadernos del Laboratorio Xeolóxico de Laxe, 8, 283–314.

López-Guijarro, R. 2006. Ambiente geodinámico y procedencia de las rocas sedimentarias precámbricas de las zonas de Ossa Morena y Centroibérica a través del análisis geoquímico. Boletín Geológico y Minero, 117, 499-505.

López-Guijarro, R., Armendáriz, M., Quesada, C., Fernández-Suárez, J., Murphy, J.B., Pin, C. and Bellido, F. 2008. Ediacaran-Palaeozoic tectonic evolution of the Ossa Morena and Central Iberian zones (SW Iberia) as revealed by Sm-Nd isotope systematics. Tectonophysics, 461, 202-214.

Lugmair, G.W. and Marti, K. 1978. Lunar initial $^{143}Nd/^{144}Nd$: differential evolution of the lunar crust and mantle. Earth and Planetary Science Letters, 39, 349–357.

Ma, B., Tian, W., Wu, G., Nance, R. D., Zhao, Y., Chen, Y. and Huang, S. 2022. The subduction-related the Great Unconformity in the Tarim intracraton, NW China. Global and Planetary Change, 215, 103883.

Macpherson, C.G., Dreher, S.T. and Thirlwall, M.F. 2006. Adakites without slab melting: High pressure differentiation of island arc magma, Mindanao, the Philippines. Earth and Planetary Science Letters, 243, 581–593.

Martin, H. 1986. Effect of steeper Archean geothermal gradient on geochemistry of subduction-zone magmas. Geology, 14, 753–756.

Martin, H., Smithies, R.H., Rapp, R., Moyen, J.F. and Champion, D. 2005. An overview of adakite, tonalite–trondhjemite–granodiorite (TTG), and sanukitoid: relationships and some implications for crustal evolution. Lithos, 79, 1–24.

Martínez Catalán, J.R. 2011. Are the oroclines of the Variscan belt related to late Variscan strike-slip tectonics? Terra Nova, 23, 241–247.

Martínez Poyatos, D.J. 1998. La estructura del borde meridional de la Zona Centroibérica (Macizo Ibérico) en el Norte de la Provincia de Córdoba. Revista de la Sociedad Geológica de España, 11, 87-94.

McDonough, W.F. and Sun, S.S. 1995. The composition of the earth. Chemical Geology, 120, 223–253.

Meert, J.G. 2003. A synopsis of events related to the assembly of eastern Gondwana. Tectonophysics, 362, 1-40.

Mitchell, R.N., Spencer, C.J., Kirscher, U., He, X.-F., Murphy, J.B., Li, Z.-X. and Collins, W.J. 2019. Harmonic hierarchy of mantle and lithospheric convective cycles: time series analysis of hafnium isotopes of zircon. Gondwana Research, 75, 239–248.

Moradi, A., Shabanian, N., Davoudian, A.R., Azizi, H., Santos, J.F. and Asahara, Y. 2022. Geochronology and petrogenesis of the Late Neoproterozoic granitic gneisses of Golpayegan metamorphic complex: a new respect for Cadomian crust in the Sanandaj-Sirjan zone, Iran. International Geology Review, 64, 1450-1473.

Murphy, J.B., Eguiluz, L. and Zulauf, G. 2002. Cadomian orogens, peri-Gondwanan correlatives and Laurentia-Baltica connections. Tectonophysics, 352, 1–9.

Nance, R.D., Murphy, J.B. and Keppie, J.D. 2002. A Cordilleran model for the evolution of Avalonia. Tectonophysics, 352, 11–31.

Nier, A. 1938. Isotopic constitution of Sr, Ba, Bi, Tl and Hg. Physical Review, 54, 275–278.

Nouri, F., Davoudian, A. R., Shabanian, N., Allen, M. B., Asahara, Y.,Azizi, H.,Anma, R., Khodami, M. and Tsuboi, M. 2022. Tectonic transition from Ediacaran continental arc to early Cambrian rift in the NE Ardakan region, central Iran: Constraints from geochronology and geochemistry of magmatic rocks. Journal of Asian Earth Sciences, 224, 105011.

O'Nions, R.K., Carter, S.R., Evensen, N.M. and Hamilton, P.J. 1979. Geochemical and cosmochemical applications of Nd isotope analysis. Annual Review of Earth and Planetary Sciences, 7, 11–38.

Ordóñez-Casado, B. 1998, Geochronological studies of the Pre-Mesozoic basement of the Iberian Massif: the Ossa Morena zone and the Allochthonous Complexes within the Central Iberian zone. PhD. Thesis, Swiss Federal Institute of Technology, Zürich, 235 p.

Parolari, M., Gómez-Tuena, A., Errázuriz-Henao, C. and Cavazos-Tovar, J.G. 2021. Orogenic andesites and their link to the continental rock cycle. Lithos, 382, 105958.

Pearce, J.A. 1982. Trace element characteristics of lavas from destructive plate boundaries. In: Thorpe, R.S., (Ed.). Andesites: Orogenic Andesites and Related Rocks. John Wiley and Sons, Chichester, 525–548.

Pearce, J.A. 1996a. A user's guide to basalt discrimination diagrams. Geological Association Canada Short Course Notes, 12, 79–113.

Pearce, J.A. 1996b. Sources and settings of granitic rocks. Episodes, 19, 120–125.

Pearce, J.A., Harris, N.B.W. and Tindle, A.G. 1984. Trace element discrimination diagrams for the tectonic interpretation of granitic rocks. Journal of Petrology, 25, 956–983.

Pearce, J.A. 2008. Geochemical fingerprinting of oceanic basalts with applications to ophiolite classification and the search for archean oceanic crust. Lithos, 100, 14– 48.

Pearce, J.A. 2014. Ophiolites: immobile elements fingerprinting of ophiolites. Elements, 10, 101–108.

Pereira, M.F. 2015. Potential sources of Ediacaran strata of Iberia: a review. Geodinamica. Acta, 27, 1–14.

Pérez Lorente, F. 1979. Geología de la zona Ossa-Morena, al norte de Córdoba (Pozoblanco-Bélmez-Villaviciosa de Córdoba). PhD. Thesis, Universidad de Granada, España, 330 pp.

Quesada, C. 1990. Precambrian successions in SW Iberia: their relationships to Cadomian orogenic events. In: D'Lemos, R.S., Strachan, R.A., Topley, C.G. (Eds.), The Cadomian Orogeny. Geological Society, London, Special Publication, 51, 353–362.

Rey, P.F. and Müller, R.D. 2010. Fragmentation of active continental plate margins owing to the buoyancy of the mantle wedge: Nature Geoscience, 3, 257–261.

Rodríguez Fernández, L.R., López Olmedo, J.T., Oliverira, T., Medialdea, P., Terrinha, P., Matas, J., Martín-Serrano, A., Martín Parra, L.M., Rubio, F., Marín, C., Montes, M. and Nozal, F. 2014. Mapa geológico de España y Portugal E: 1.1000.000. Instituto geológico y Minero de España, Madrid.

Rojo-Pérez, E., Arenas, R., Fuenlabrada, J.M., Sánchez Martínez, S., Martín Parra, L.M., Matas, J., Pieren, A.P. and Díez Fernández, R. 2019. Contrasting isotopic sources (Sm-Nd) of Late Ediacaran series in the Iberian Massif: implications for the Central Iberian-Ossa Morena boundary. Precambrian Research, 324, 194–207.

Rojo-Pérez, E., Fuenlabrada, J.M., Linnemann, U., Arenas, R., Sánchez Martínez, S., Díez Fernández, R., Martín Parra, L.M., Matas, J., Andonaegui, P. and Fernández- Suárez, J. 2021. Geochemistry and Sm–Nd isotopic sources of Late Ediacaran siliciclastic series in the Ossa-Morena Complex: Iberian-Bohemian correlations. International Journal of Earth Sciences, 110, 467–485.

Rojo-Pérez, E., Linnemann, U., Hofmann, M., Fuenlabrada, J.M., Zieger, J., Fernández-Suárez, J., Andonaegui, P., Sánchez Martínez, S., Díez Fernández, R., and Arenas, R. 2022. U-Pb geochronology and isotopic geochemistry of adakites and related magmas in the well-preserved Ediacaran arc section of the SW Iberian Massif: the role of subduction erosion cycles in peri-Gondwanan arcs. Gondwana Research, 109, 89-112.

Sánchez-Carretero, R., Carracedo, M., Eguíluz, L., Garrote, A. and Apalategui, O. 1989. El magmatismo calcoalcalino del Precámbrico terminal en la Zona de Ossa Morena (Macizo Ibérico). Revista de la Sociedad Geológica de España, 7-21.

Sánchez-Carretero, R., Eguiluz, L., Pascual, E. and Carracedo, M. 1990. Ossa-Morena Zone: igneous rocks. In: Dallmeyer, R.D., Martínez García, E., (Eds.), Pre-Mesozoic Geology of Iberia. Springer-Verlag, Berlin, 292–313 pp.

Sánchez-García, T., Bellido, F., Pereira, M.F., Chichorro, M., Quesada, C., Pin, C. and Silva, J.B. 2010. Rift-related volcanism predating the birth of the Rheic Ocean (Ossa-Morena zone, SW Iberia). Gondwana Research, 17, 392–407.

Sánchez-Lorda, M.E., Ábalos, B., García de Madinabeitia, S., Eguiluz, L., Gil Ibarguchi, J.I. and Paquette, J.L. 2016. Radiometric discrimination of pre-Variscan amphibolites in the Ediacaran Serie Negra (Ossa- Morena Zone, SW Iberia). Tectonophysics, 681, 3145.

Sarrionandia, F., Carracedo-Sánchez, M., Eguiluz, L., Ábalos, B., Rodríguez, J., Pin, C. and Gil Ibarguchi, J.I. 2012. Cambrian rift-related magmatism in the Ossa-Morena Zone (Iberian Massif): Geochemical and geophysical evidence of Gondwana break-up. Tectonophysics, 570-571, 135–150.

Sarrionandia, F., Ábalos, B., Errandonea-Martin, J., Eguíluz, L., Santos-Zalduegui, J.F., García de Madinabeitia, S., Carracedo-Sánchez, M. and Gil Ibarguchi, J.I. 2020. Ediacaran - Earliest Cambrian arc-tholeiite and adakite associations of the Malcocinado Formation (Ossa-Morena Zone, SW Spain): Juvenile continental crust and deep crustal reworking in northern Gondwana. Lithos, 372–373, 105683.

Schäfer, H.J., Gebauner, D., Nägler, T.F. and Eguiluz, L. 1993. Conventional and ionmicroprobe U-Pb dating of detrital zircons of the Tentudia Group (Serie Negra, SW Spain): implications for zircon systematics, stratigraphy, tectonics and the Precambrian/Cambrian boundary. Contributions to Mineralogy and Petrology, 113, 289–299.

Shand, S.J. 1943. The eruptive rocks: 2nd edition, John Wiley, New York, 444 p.

Skjerlie, K.P. and Johnston, A.D. 1993. Fluid-absent melting behavior of an F-rich tonalitic gneiss at mid-crustal pressures: Implications for the generation of anorogenic granites. Journal of Petrology, 34, 785-815.

Sun, S.S. and McDonough, W.F. 1989. Chemical and isotopic systematics of oceanic basalts: implications for mantle composition and processes. In: Saunders, A.D., Norry, M.J., (Eds.). Magmatism in the ocean basins. Geological Society, London, Special Publications, 42, 315-345.

Stern, R.J. 1994. Arc-assembly and continental collision in the Neoproterozoic African orogen: implications for the consolidation of Gondwanaland. Annual Review of Earth and Planetary Sciences, 22, 319-351.

Stern, C.R. 2020. The role of subduction erosion in the generation of Andean and other convergent plate boundary arc magmas, the continental crust and mantle. Gondwana Research, 88, 220–249.

Tanaka, T., Togashi, S., Kamioka, H., Amakawa, H., Kagami, H., Hamamoto, T., Yuhara, M., Orihashi, Y., Yoneda, S., Shimizu, H., Kunimaru, T., Takahashi, K., Yanagi, T., Nakano, T., Fujimaki, H., Shinjo, R., Asahara, Y., Tanimizu, M. and Dragusanu, C. 2000. JNdi-1: a neodymium isotopic reference in consistency with LaJolla neodymium. Chemical Geology, 168, 279–281.

Von Raumer, J.F., Stampfli, G.M., Arenas, R. and Sánchez Martínez, S. 2015. Ediacaran to Cambrian oceanic rocks of the Gondwana margin and their tectonic interpretation. International Journal of Earth Sciences, 104, 1107–1121.

White, W.M. 2015. Isotope Geochemistry. Wiley-Blackwell, 496 p.

Winchester, J.A. and Floyd, P.A. 1977. Geochemical Discrimination of Different Magma Series and Their Differentiation Product Using Immobile Elements. Chemical Geology, 20, 325–343.

Wood, D.A. 1980. The application of a Th-Hf-Ta diagram to problems of tectonomagmatic classification and to establishing the nature of crustal contamination of basaltic lavas of the British Tertiary volcanic province. Earth and Planetary Science Letters, 50, 11–30.

Figure captions

Figure 1. Zonation of the Variscan Orogen (Díez Fernández and Arenas, 2015; Arenas et al. 2016), based on Franke (1989) and Martínez Catalán (2011). Location of the geological map shown in Fig. 2a is marked by the dashed polygon.

Figure 2. (a) Geological map of the Ossa–Morena Complex and the southern part of the Central Iberian Zone, based on the 1:1.000.000 geological map of Spain and Portugal (Rodríguez Fernández et al. 2014; Rojo-Pérez

et al. 2019). Location of the study area is marked by a rectangle. (b) Schematic stratigraphic column of the Malcocinado Formation.

Figure 3. Pictures showing field aspects of the metabreccias, metavolcanics and metaconglomerates of the Malcocinado Formation. (a) Andesitic breccias. (b) Angular rock fragments with cooling rims in metabreccias. (c) Metadacite-metarhyolite layer with 1 cm quartz crystals. (d) Volcanic glass preserved in a flame structure within a metadacite-metarhyolite layer. (e) and (f) Clast-supported conglomerate with well-rounded clasts of granites and volcanic rocks, surrounded by detrital matrix.

Figure 4. Microscope images of andesites and metagranites of the Malcocinado Formation. (a) Flow texture in metaandesite (XPL), with microcrystalline matrix and plagioclase phenocrysts. (b) Metaandesite with autolytic microbrecciation (PPL); note the idiomorphic plagioclase pseudomorphs. (c) Intergrowth (graphic) texture in metagranite (XPL). (d) General texture of a metagranite (XPL); note the graphic textures, partially saussuritized plagioclase and potassium feldspar, and chloritized biotites.

Figure 5. (a) Zr/Ti - Nb/Y diagram (Pearce, 1996a) showing the classification of the Malcocinado Formation metaigneous rocks. (b) Th-Co diagram (Hastie et al. 2007) for the Malcocinado Formation metavolcanites. (c) and (d) Fe-number vs. SiO_2 diagram and MALI-index vs. SiO_2 diagram (after Frost et al. 2001), respectively, of the Malcocinado Formation metagranites.

Figure 6. (a) and (b) Chondrite-normalized REE patterns (Sun and McDonough, 1989) of the Malcocinado Formation samples. (c) and (b) Multivariate trace element patterns normalized to the Primitive Mantle (after McDonough and Sun, 1995) of the Malcocinado Formation samples.

Figure 7. (a) $(La/Yb)_N$-Yb_N discrimination diagrams for adakite-like rocks and common volcanic-arc magmas (Defant and Drummond, 1990; MacPherson et al. 2006). (b) Th/Yb - Nb/Yb diagram (Pearce, 2008, 2014) for the Malcocinado Formación. SSZ, Supra-Subduction Zone; N-MORB, Normal-Mid Oceanic Ridge Basalts; E-MORB, Enriched- Mid Oceanic Ridge Basalts; OIB, Ocean Island Basalts. (c) Tectonic setting discrimination diagram for metagranites (Pearce et al. 1984). Dotted regions represent areas for Chilean and Alaskan arc batholiths. ORG, Ocean-Ridge Granitoids; syn-COLG, Syncollisional Granitoids; post-COLG,

Postcollisional Granitoids; VAG, Volcanic-Arc Granitoids; WPG, Within-Plate Granitoids. (d) Hf-Th-Nb discrimination diagram (Wood, 1980). A, N-MORB; B, E-MORB and Within-Plate Tholeiites; C, Within-Plate Alkaline Basalts; D, Volcanic-Arc Basalts, the dashed line separates the Island-Arc Tholeiites (Hf/Th > 3) from the Calc-Alkaline Basalts (Hf/Th < 3).

Figure 8. (a) εNd vs. age diagram showing TDM values for Early Paleozoic Malcocinado Formation metaigneous rocks. The range of Nd model ages obtained by Sarrionandia et al. (2020), as well as those of the Montemolín metabasites and metagranitic complexes of the Mérida Massif (Rojo-Pérez et al. 2022) are also shown. (b) $\varepsilon Nd_{(t)}$ vs. $^{87}Sr/^{86}Sr_{(t)}$ diagram for the rocks belonging to the Malcocinado Formation. Values of Montemolín metabasites and Mérida Massif metagranitic complexes appear gathered in green and red areas, respectively. The relative location of the continental crust and enriched mantle type I (EM I) and type II (EMII) are shown. Red and green arrows show the mixing paths calculated by Castro et al. (2021) for Andean batholiths.

Figure 9. Simplified model for the (Early Cambrian) mature stage of the continental arc section preserved in the Ossa-Morena Complex. Early Cambrian arc collapse and erosion before the onset of a tectonic switch affecting the North-African Gondwana margin. Magmatic events occurred between pre.-602 and 541 Ma are described in Rojo Pérez et al. (2022).

table

Table 1 Coordinates of the Malcocinado Formation rocks.

	Latitude	Longitude
Metadacites and Metarhyolites		
MAL-01	38º 06' 06''	-5º 42' 45''
MAL-02	38º 06' 25''	-5º 42' 20''
MAL-03	38º 06' 25''	-5º 42' 20''
MAL-11	38º 05' 40''	-5º 43' 57''
Metaandesites		
MAL-04	38º 06' 25''	-5º 42' 20''
MAL-05	38º 06' 25''	-5º 42' 20''
MAL-10	38º 05' 40''	-5º 43' 57''
MAL-12	38º 05' 40''	-5º 43' 57''
MAL-13	38º 05' 40''	-5º 43' 57''
MAL-14	38º 08' 30''	-5º 49' 20''
Metagranitoids		
MAL-06	38º 05' 55''	-5º 43' 05''
MAL-07	38º 05' 55''	-5º 43' 05''
MAL-08	38º 05' 55''	-5º 43' 37''
MAL-09	38º 05' 55''	-5º 43' 37''

table

Table 2 Whole-rock major and trace elements of the Malcocinado Formation

	Metadacites and metarhyolites				Metaandesites						Metagranites			
	MAL-01	**MAL-02**	**MAL-03**	**MAL-11**	**MAL-04**	**MAL-05**	**MAL-10**	**MAL-12**	**MAL-13**	**MAL-14**	**MAL-06**	**MAL-07**	**MAL-08**	**MAL-09**
SiO_2	80.44	66.5	68.24	59.35	52.37	60.55	56.49	52.51	57.16	52.15	68.96	70.79	69.57	67.27
TiO_2	0.074	0.361	0.334	1.001	0.85	0.578	0.909	1.034	0.919	0.484	0.242	0.268	0.263	0.28
Al_2O_3	10.53	17.45	16.76	16.72	17.98	16.27	16.94	18.36	17.28	15.01	14.52	14.93	16.11	15.2
$Fe_2O_{3(T)}$	1.95	4.72	4.41	7.79	7.18	7.53	9.48	9.65	7.65	8.39	2.97	2.28	2.3	2.47
FeO	1.75	4.25	3.97	7.01	6.46	6.78	8.53	8.68	6.88	7.55	2.67	2.05	2.07	2.22
MnO	0.016	0.012	0.016	0.163	0.134	0.126	0.188	0.155	0.164	0.236	0.048	0.045	0.054	0.087
MgO	0.63	0.59	0.47	4.22	2.77	2.27	2.79	5.13	4.14	8.53	0.62	0.44	0.41	0.49
$FeO_{(t)}$/MgO	2.79	7.20	8.44	1.66	2.33	2.98	3.06	1.69	1.66	0.89	4.31	4.66	5.05	4.54
CaO	0.05	0.19	0.15	0.85	4.24	1.97	1.33	1.31	1.47	4.44	1.22	1.07	0.98	3.15
Na_2O	0.29	2.86	2.8	3.68	4.03	3.47	7.76	5.06	5.74	3.1	3.83	3.97	2.81	3.4
K_2O	3.78	5.66	5.38	2.64	3.66	3.85	0.32	2	1.34	0.14	4.24	4.82	5.66	4.56
P_2O_5	< 0.01	0.1	0.06	0.28	0.26	0.22	0.21	0.23	0.28	0.18	0.07	0.09	0.09	0.09
LOI	1.91	2.04	1.91	3.54	5.47	3.38	2.15	3.54	3.15	7.16	1.98	1.81	2.21	3.47
Total	99.67	100.5	100.5	100.2	98.94	100.2	98.58	98.99	99.3	99.84	98.69	100.5	100.5	100.5
MgO/MgO+FeO	0.26	0.12	0.11	0.38	0.30	0.25	0.25	0.37	0.38	0.53	0.19	0.18	0.17	0.18
A/CKN	2.56	2.00	2.01	2.33	1.51	1.75	1.80	2.19	2.02	1.95	1.56	1.51	1.70	1.37
AI	13.03	1.98	1.92	0.72	0.91	1.11	0.04	0.40	0.23	0.05	1.11	1.21	2.01	1.34
Cs	3.7	5.7	5.3	3.2	6.6	7.6	0.3	2.2	1.5	0.1	1.3	1.3	2.4	2.2
Ba	719	1312	1348	578	622	1051	229	419	345	84	910	898	932	752
Rb	119	146	153	98	120	127	9	76	50	2	98	104	148	134
Sr	9	91	87	163	293	230	269	246	266	78	99	88	60	100
Nb	6.2	9.9	10.4	9.1	5.4	4.5	3.9	5.4	5	1.5	12.4	12.5	14.4	15.9
Hf	3.5	6.3	6.6	10.7	3.8	3.6	2.7	4.1	3.8	1.6	6.8	5.7	6.2	7.3
Zr	121	250	252	418	151	145	99	154	139	57	276	258	242	261
Y	27	33.1	27.4	32.8	33	18.7	23.4	29.9	26.7	15.8	35.6	31	30.3	38.2
Pb	< 5	6	8	< 5	11	< 5	7	8	5	< 5	8	5	9	9
Th	13.3	16.3	15	8.36	1.97	2.51	1.52	2.62	2.49	1.48	25	22.9	27	31.2
U	4.65	4.69	5.14	1.79	0.74	0.7	0.73	1.01	1.04	0.42	6.35	6.72	6.89	9.72

Cr	< 20	< 20	< 20	110	< 20	50	< 20	20	< 20	100	< 20	< 20	< 20	< 20
Ni	< 20	< 20	< 20	< 20	< 20	< 20	< 20	< 20	< 20	30	< 20	< 20	< 20	< 20
Co	3	5	11	22	20	17	20	26	25	26	12	24	18	16
V	8	9	6	154	167	150	167	179	139	126	17	15	19	18
Sc	5	15	13	19	16	11	19	20	18	27	6	6	6	6
Ga	13	20	19	19	20	19	15	20	17	16	15	14	16	17
Sr/Y	0.33	2.75	3.18	4.97	8.88	12.30	11.50	8.23	9.96	4.94	2.78	2.84	1.98	2.62
Ba/Th	54.06	80.49	89.87	69.14	315.74	418.73	150.66	159.92	138.55	56.76	36.40	39.21	34.52	24.10
Th/Ta	23.33	23.62	20.00	10.72	4.93	6.61	5.63	6.09	6.23	11.38	20.83	20.63	20.61	23.11
Ce/Yb	14.84	31.16	27.57	17.05	6.67	10.71	9.71	11.20	10.61	11.87	27.03	29.46	34.06	28.32
La	22.7	67.6	52.6	27.6	12.5	11.9	12.5	17.3	14.6	8.62	59.5	55.8	67.3	76.3
Ce	50.3	129	102	61.9	22.6	24.1	23.2	33.6	33.2	17.8	110	104	125	143
Pr	5.43	15	11.6	7.09	3.4	3.44	3.97	4.83	4.36	2.51	12.1	11.6	13.4	15.6
Nd	20.5	56.2	43.2	28.8	14.9	14.7	18.1	20.2	18.7	11.2	43	41.7	47.6	55.2
Sm	4.31	10.3	8.09	5.84	3.79	3.13	4.38	4.85	4.58	2.69	8.17	7.44	8.06	9.8
Eu	0.641	1.82	1.58	1.53	1.05	0.662	1.33	1.4	1.3	0.757	1.27	1.13	1.37	1.61
Gd	3.76	8.19	6.12	5.74	4.26	2.87	4.53	4.83	4.66	2.72	6.32	5.81	6.09	7.55
Tb	0.66	1.1	0.91	0.94	0.78	0.47	0.76	0.84	0.78	0.44	0.97	0.91	0.9	1.13
Dy	4.49	6.24	4.98	5.91	5.3	3.05	4.55	5.19	4.89	2.63	5.95	5.41	5.23	6.62
Ho	1	1.28	1.02	1.21	1.19	0.67	0.9	1.06	1.04	0.55	1.23	1.1	1.05	1.37
Er	3.17	3.84	3.28	3.57	3.54	2.25	2.59	3.09	3.2	1.6	3.65	3.29	3.17	4.22
Tm	0.473	0.577	0.521	0.529	0.524	0.338	0.368	0.463	0.46	0.225	0.577	0.511	0.504	0.667
Yb	3.39	4.14	3.7	3.63	3.39	2.25	2.39	3	3.13	1.5	4.07	3.53	3.67	5.05
Lu	0.563	0.694	0.628	0.596	0.566	0.401	0.39	0.525	0.509	0.244	0.693	0.605	0.622	0.81
Ta	0.57	0.69	0.75	0.78	0.4	0.38	0.27	0.43	0.4	0.13	1.2	1.11	1.31	1.35
Eu/Eu*	0.16	0.20	0.22	0.26	0.26	0.22	0.30	0.29	0.28	0.28	0.18	0.17	0.20	0.19
LaN/YbN	4.80	11.71	10.20	5.45	2.64	3.79	3.75	4.14	3.35	4.12	10.49	11.34	13.15	10.84
GdN/YbN	0.92	1.64	1.37	1.31	1.04	1.06	1.57	1.33	1.23	1.50	1.28	1.36	1.37	1.24
sumREE	120.82	305.29	239.60	154.29	77.22	69.83	79.57	100.65	94.90	53.24	256.81	242.23	283.34	328.12
LREEN	307.20	841.57	656.09	392.07	182.14	177.74	199.83	253.69	231.72	133.44	703.64	665.40	783.87	902.07
HREEN	129.55	201.92	163.93	166.04	145.22	92.42	124.45	142.67	140.37	75.27	177.80	160.99	162.39	209.26
LREE/HREE	2.37	4.17	4.00	2.36	1.25	1.92	1.61	1.78	1.65	1.77	3.96	4.13	4.83	4.31

LaN/SmN	3.40	4.24	4.20	3.05	2.13	2.45	1.84	2.30	2.06	2.07	4.70	4.84	5.39	5.03
dm (LaN/YbN)	33.82	52.78	49.84	36.52	21.12	28.80	28.56	30.64	26.13	30.57	50.43	52.09	55.25	51.13
dm (Sr/Y)	8.42	11.10	11.57	13.57	17.91	21.70	20.81	17.18	19.11	13.53	11.14	11.20	10.25	10.96
La/Sm	5.27	6.56	6.50	4.73	3.30	3.80	2.85	3.57	3.19	3.20	7.28	7.50	8.35	7.79
Ba/La	31.67	19.41	25.63	20.94	49.76	88.32	18.32	24.22	23.63	9.74	15.29	16.09	13.85	9.86
Nb/Zr	0.05	0.04	0.04	0.02	0.04	0.03	0.04	0.04	0.04	0.03	0.04	0.05	0.06	0.06

table

Table 3 **Whole-rock Isotopic Sr-Nd data of the Malcocinado Formation.**

	Sample	Sm	Nd	Sm/Nd	$^{147}Sm/^{144}Nd$	$^{143}Nd/^{144}Nd$	±StErr*10-6	$^{(b)}T_{DM}$	$\varepsilon Nd_{(0)}$	$^{(a)}\varepsilon Nd_{(t)}$	$f_{Sm/Nd}$	$^{143}Nd/^{144}Nd_{(t)}$
Metadacites and metarhyolites	**MAL_01**	4.31	20.5	0.210	0.1271	0.512430	2	1082	-4.1	0.7	-0.35	0.511985
	MAL_02	10.3	56.2	0.183	0.1108	0.512358	2	1019	-5.5	0.4	-0.44	0.511970
	MAL_03	8.09	43.2	0.187	0.1132	0.512396	1	987	-4.7	1.0	-0.42	0.512000
	MAL_11	5.84	28.8	0.203	0.1226	0.512199	1	1410	-8.6	-3.5	-0.38	0.511770
Metaandesites	**MAL_04**	3.79	14.9	0.254	0.1538	0.512627	1	1061	-0.2	2.7	-0.22	0.512089
	MAL_05	3.13	14.7	0.213	0.1287	0.512555	1	883	-1.6	3.0	-0.35	0.512105
	MAL_10	4.38	18.1	0.242	0.1463	0.512555	1	1104	-1.6	1.8	-0.26	0.512044
	MAL_12	4.85	20.2	0.240	0.1451	0.512489	4	1230	-2.9	0.6	-0.26	0.511982
	MAL_13	4.58	18.7	0.245	0.1481	0.512493	1	1274	-2.8	0.5	-0.25	0.511975
	MAL_14	2.69	11.2	0.240	0.1452	0.512462	1	1290	-3.4	0.1	-0.26	0.511954
Metagranites	**MAL_06**	8.17	43.0	0.190	0.1149	0.512426	1	957	-4.1	1.4	-0.42	0.512024
	MAL_07	7.44	41.7	0.178	0.1079	0.512408	3	921	-4.5	1.6	-0.45	0.512030
	MAL_08	8.06	47.6	0.169	0.1024	0.512435	3	841	-4.0	2.5	-0.48	0.512077
	MAL_09	9.80	55.2	0.178	0.1073	0.512357	2	988	-5.5	0.6	-0.45	0.511982

	Sample	Rb	Sr	Rb/Sr	$^{87}Rb/^{86}Sr$	$^{87}Sr/^{86}Sr$	±StErr*10-6	$\varepsilon Sr_{(0)}$	$\varepsilon Sr_{(t)}$	$^{37}Sr/^{86}Sr_{(t)}$
Metadacites and metarhyolites	**MAL_01**	119.00	9.00	13.22	39.096	0.932308	3	3234	-982	0.6347
	MAL_02	146.00	91.00	1.60	4.655	0.735890	2	446	-48	0.7005
	MAL_03	153.00	87.00	1.76	5.105	0.742076	2	533	-9	0.7032
	MAL_11	98.00	163.00	0.60	1.741	0.718614	2	200	21	0.7054
Metaandesites	**MAL_04**	120.00	293.00	0.41	1.186	0.713130	2	122	3	0.7041
	MAL_05	127.00	230.00	0.55	1.599	0.715682	2	159	-5	0.7035
	MAL_10	9.00	269.00	0.03	0.097	0.707573	2	44	42	0.7068
	MAL_12	76.00	246.00	0.31	0.894	0.712480	2	113	26	0.7057
	MAL_13	50.00	266.00	0.19	0.544	0.710449	2	84	35	0.7063
	MAL_14	2.00	78.00	0.03	0.074	0.707074	2	37	38	0.7065

	MAL_06	98.00	99.00	0.99	2.869	0.726169	2	308	7	0.7043
Metagranites	**MAL_07**	104.00	88.00	1.18	3.427	0.731835	2	388	27	0.7057
	MAL_08	148.00	60.00	2.47	7.169	0.754540	2	710	-55	0.7000
	MAL_09	134.00	100.00	1.34	3.887	0.733020	2	405	-6	0.7034

[a] $\varepsilon Nd_{(t)}$ calculated at 534 Ma (Sarrionandi et al., 2020) for the Malcocinado Formation.

[b] Nd model ages (DePaolo, 1981)

Decay constant for ^{147}Sm: 6.54 × 10–12 years−1 (Lugmair and Marti, 1978)

CHUR current parameters: $^{147}Sm/^{144}Nd$ = 0.1967; $^{143}Nd/^{144}Nd$ = 0.512638 (Jacobsen and Wasserburg, 1980)

figure

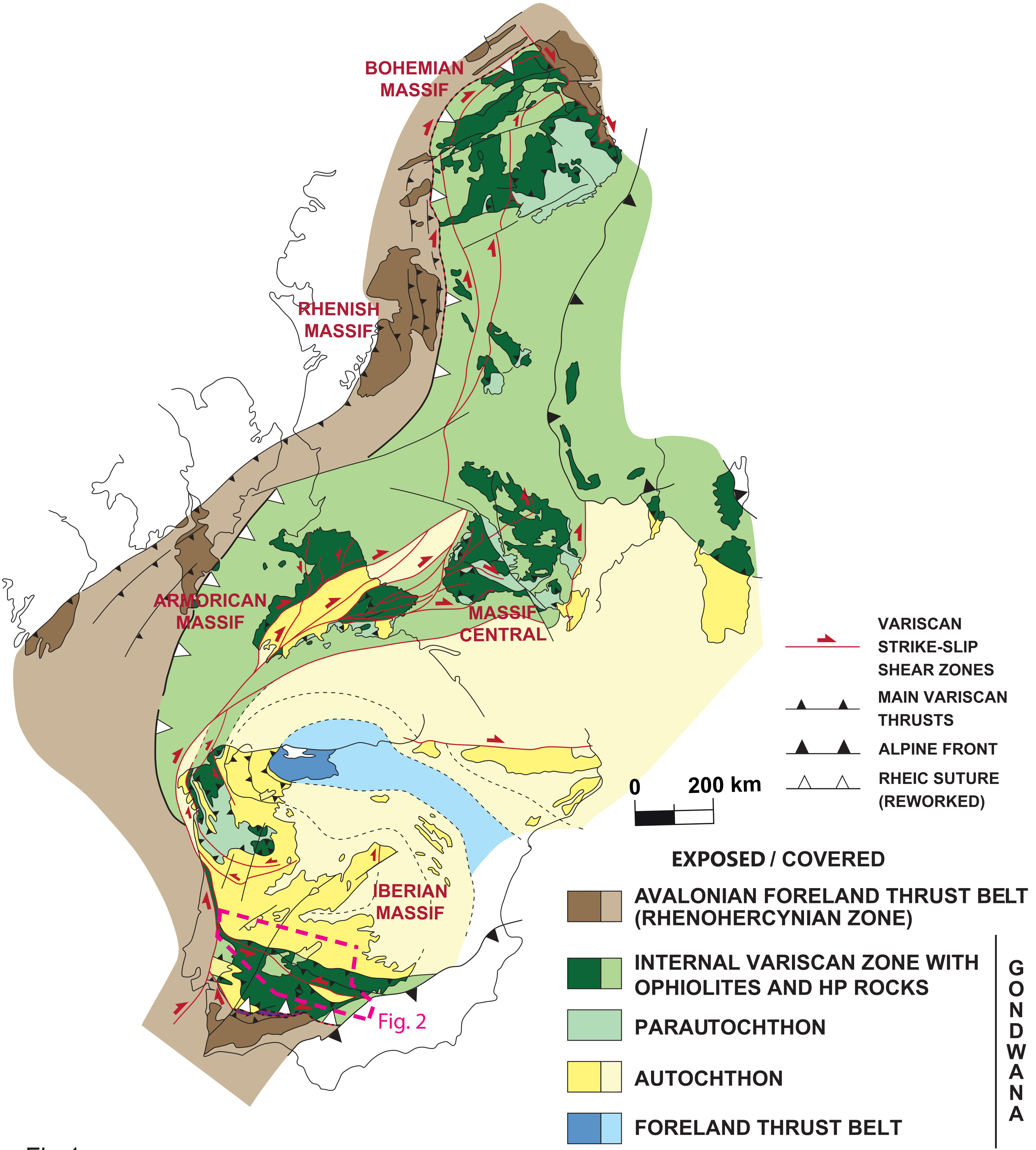
BOHEMIAN
MASSIF
RHENISH
MASSIF
ARMORICAN
MASSIF
MASSIF
CENTRAL
IBERIAN
MASSIF
Fig. 2
0
200 km
VARISCAN
STRIKE-SLIP
SHEAR ZONES
MAIN VARISCAN
THRUSTS
ALPINE FRONT
RHEIC SUTURE
(REWORKED)
EXPOSED / COVERED
AVALONIAN FORELAND THRUST BELT
(RHENOHERCYNIAN ZONE)
INTERNAL VARISCAN ZONE WITH
OPHIOLITES AND HP ROCKS
PARAUTOCHTHON
AUTOCHTHON
FORELAND THRUST BELT
GONDWANA

Fig.1

figure

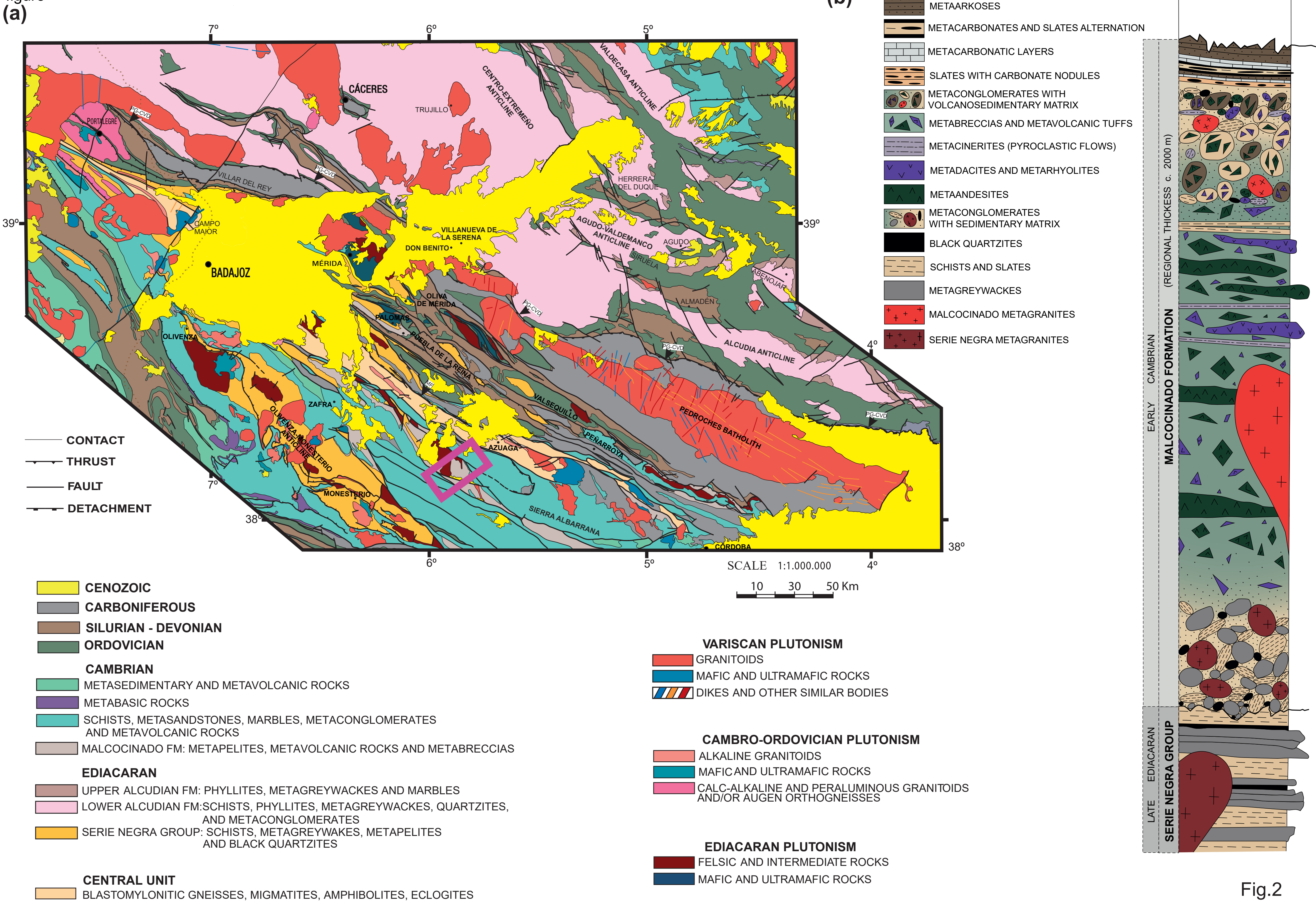
(a)
(b)
7°
6°
5°
4°
39°
38°
CÁCERES
TRUJILLO
PORTALEGRE
PG-CVD
VILLAR DEL REY
CENTRO-EXTREMEÑO ANTICLINE
VALDECASA ANTICLINE
HERRERA DEL DUQUE
CAMPO MAIOR
BADAJOZ
MÉRIDA
VILLANUEVA DE LA SERENA
DON BENITO
AGUDO-VALDEMANCO ANTICLINE
AGUDO
SIRUELA
ABENOJAR
ALMADÉN
OLIVA DE MÉRIDA
PALOMAS
PUEBLA DE LA REINA
ALCUDIA ANTICLINE
OLIVENZA
ZAFRA
VALSEQUILLO
PEDROCHES BATHOLITH
OLIVENZA-MONESTERIO ANTICLINE
AZUAGA
PEÑARROYA
MONESTERIO
SIERRA ALBARRANA
CÓRDOBA
CONTACT
THRUST
FAULT
DETACHMENT
SCALE 1:1.000.000
10 30 50 Km
CENOZOIC
CARBONIFEROUS
SILURIAN - DEVONIAN
ORDOVICIAN
CAMBRIAN
METASEDIMENTARY AND METAVOLCANIC ROCKS
METABASIC ROCKS
SCHISTS, METASANDSTONES, MARBLES, METACONGLOMERATES AND METAVOLCANIC ROCKS
MALCOCINADO FM: METAPELITES, METAVOLCANIC ROCKS AND METABRECCIAS
EDIACARAN
UPPER ALCUDIAN FM: PHYLLITES, METAGREYWACKES AND MARBLES
LOWER ALCUDIAN FM:SCHISTS, PHYLLITES, METAGREYWACKES, QUARTZITES, AND METACONGLOMERATES
SERIE NEGRA GROUP: SCHISTS, METAGREYWAKES, METAPELITES AND BLACK QUARTZITES
CENTRAL UNIT
BLASTOMYLONITIC GNEISSES, MIGMATITES, AMPHIBOLITES, ECLOGITES
VARISCAN PLUTONISM
GRANITOIDS
MAFIC AND ULTRAMAFIC ROCKS
DIKES AND OTHER SIMILAR BODIES
CAMBRO-ORDOVICIAN PLUTONISM
ALKALINE GRANITOIDS
MAFIC AND ULTRAMAFIC ROCKS
CALC-ALKALINE AND PERALUMINOUS GRANITOIDS AND/OR AUGEN ORTHOGNEISSES
EDIACARAN PLUTONISM
FELSIC AND INTERMEDIATE ROCKS
MAFIC AND ULTRAMAFIC ROCKS
METAARKOSES
METACARBONATES AND SLATES ALTERNATION
METACARBONATIC LAYERS
SLATES WITH CARBONATE NODULES
METACONGLOMERATES WITH VOLCANOSEDIMENTARY MATRIX
METABRECCIAS AND METAVOLCANIC TUFFS
METACINERITES (PYROCLASTIC FLOWS)
METADACITES AND METARHYOLITES
METAANDESITES
METACONGLOMERATES WITH SEDIMENTARY MATRIX
BLACK QUARTZITES
SCHISTS AND SLATES
METAGREYWACKES
MALCOCINADO METAGRANITES
SERIE NEGRA METAGRANITES
EARLY CAMBRIAN
MALCOCINADO FORMATION
(REGIONAL THICKESS c. 2000 m)
LATE EDIACARAN
SERIE NEGRA GROUP

Fig.2

figure

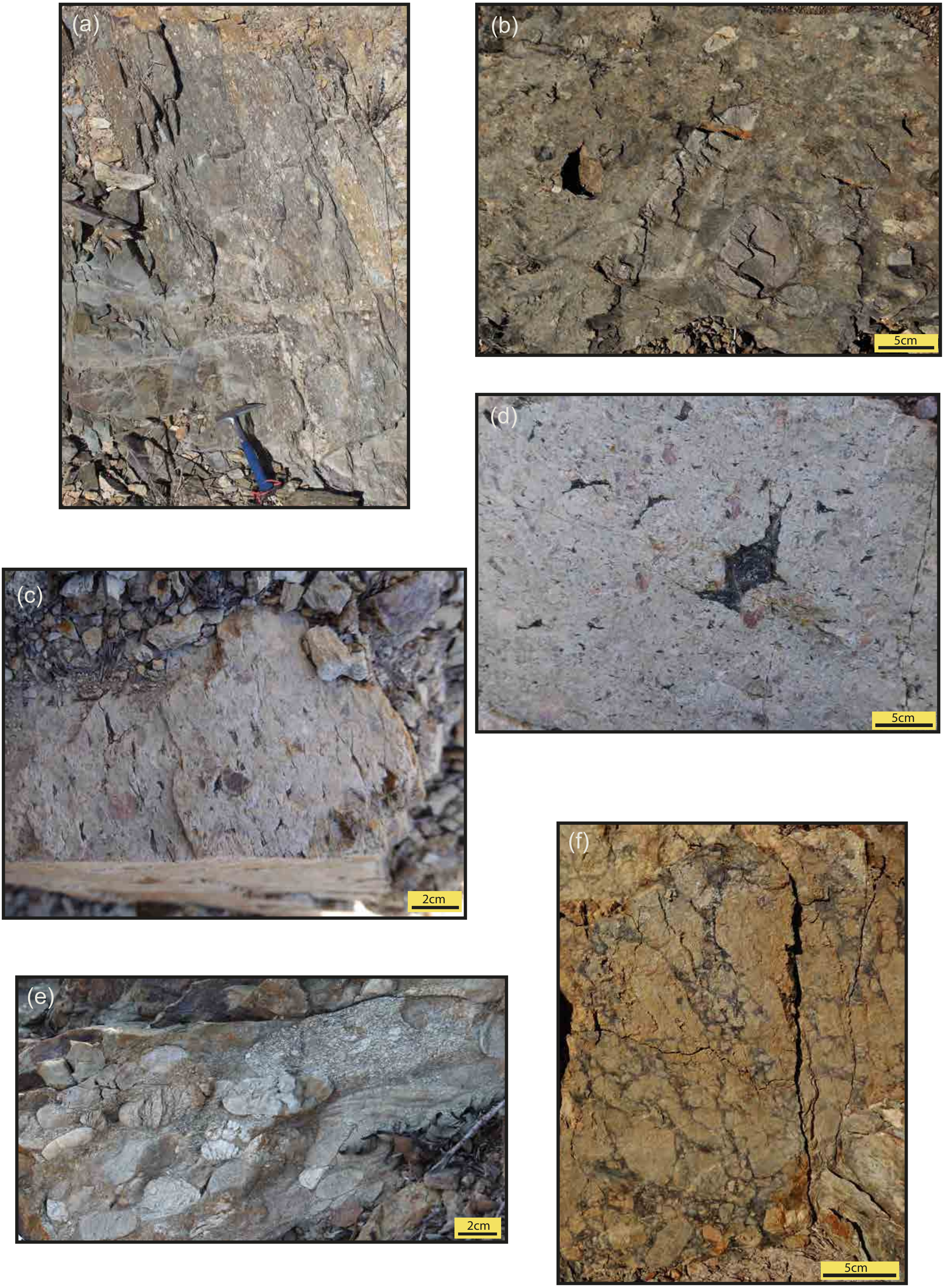

Fig.3

figure

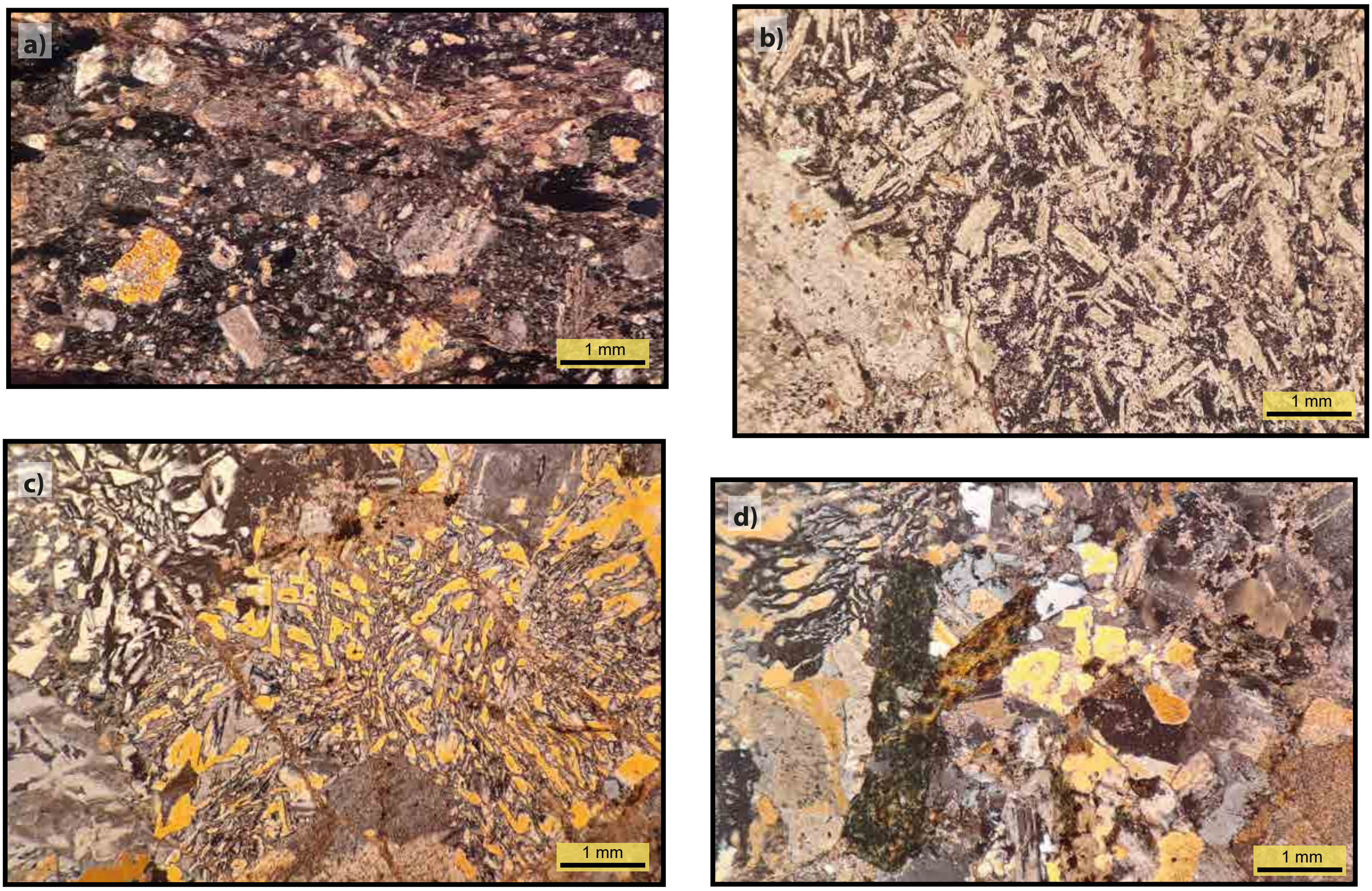

Fig.4

figure

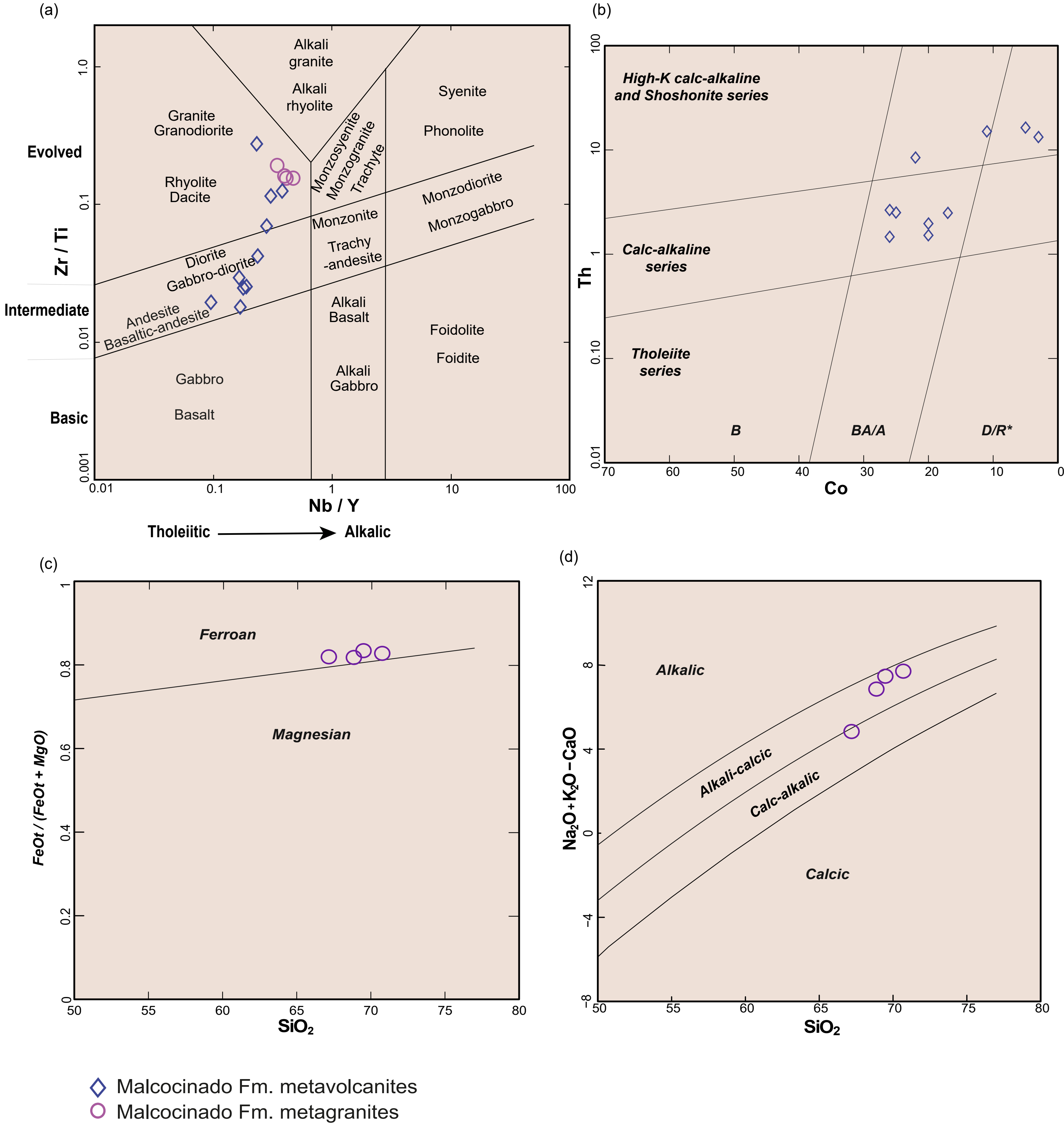
(a)
Alkali granite
Alkali rhyolite
Syenite
Phonolite
Granite Granodiorite
Evolved
Rhyolite Dacite
Monzosyenite
Monzogranite
Trachyte
Monzodiorite
Monzogabbro
Monzonite
Trachy -andesite
Diorite
Gabbro-diorite
Zr / Ti
Intermediate
Andesite
Basaltic-andesite
Alkali Basalt
Foidolite
Foidite
Gabbro
Alkali Gabbro
Basic
Basalt
Nb / Y
Tholeiitic
Alkalic
(b)
High-K calc-alkaline and Shoshonite series
Calc-alkaline series
Th
Tholeiite series
B
BA/A
D/R*
Co
(c)
Ferroan
Magnesian
FeOt / (FeOt + MgO)
SiO2
(d)
Alkalic
Alkali-calcic
Calc-alkalic
Calcic
Na2O+K2O−CaO
SiO2
Malcocinado Fm. metavolcanites
Malcocinado Fm. metagranites

Fig.5

figure

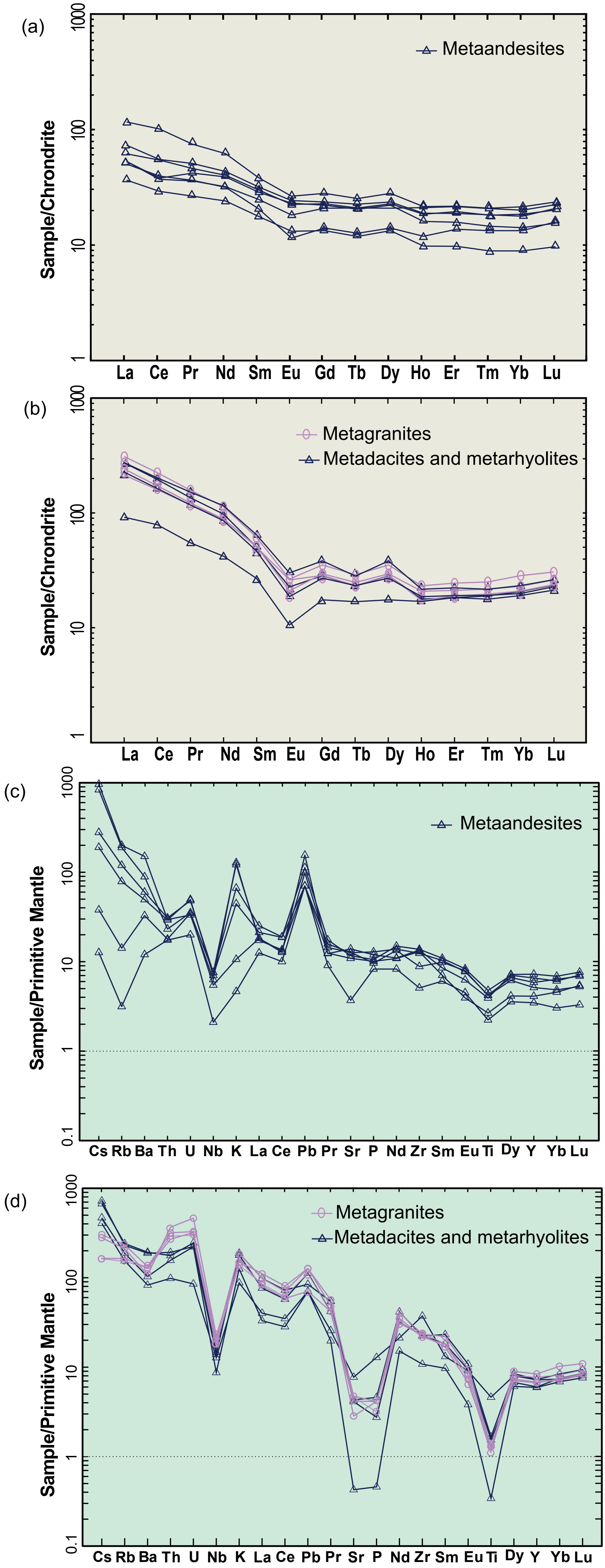

(a)
Metaandesites
Sample/Chrondrite
1000
100
10
1
La Ce Pr Nd Sm Eu Gd Tb Dy Ho Er Tm Yb Lu
(b)
Metagranites
Metadacites and metarhyolites
Sample/Chrondrite
1000
100
10
1
La Ce Pr Nd Sm Eu Gd Tb Dy Ho Er Tm Yb Lu
(c)
Metaandesites
Sample/Primitive Mantle
1000
100
10
1
0.1
Cs Rb Ba Th U Nb K La Ce Pb Pr Sr P Nd Zr Sm Eu Ti Dy Y Yb Lu
(d)
Metagranites
Metadacites and metarhyolites
Sample/Primitive Mantle
1000
100
10
1
0.1
Cs Rb Ba Th U Nb K La Ce Pb Pr Sr P Nd Zr Sm Eu Ti Dy Y Yb Lu

Fig. 6

figure

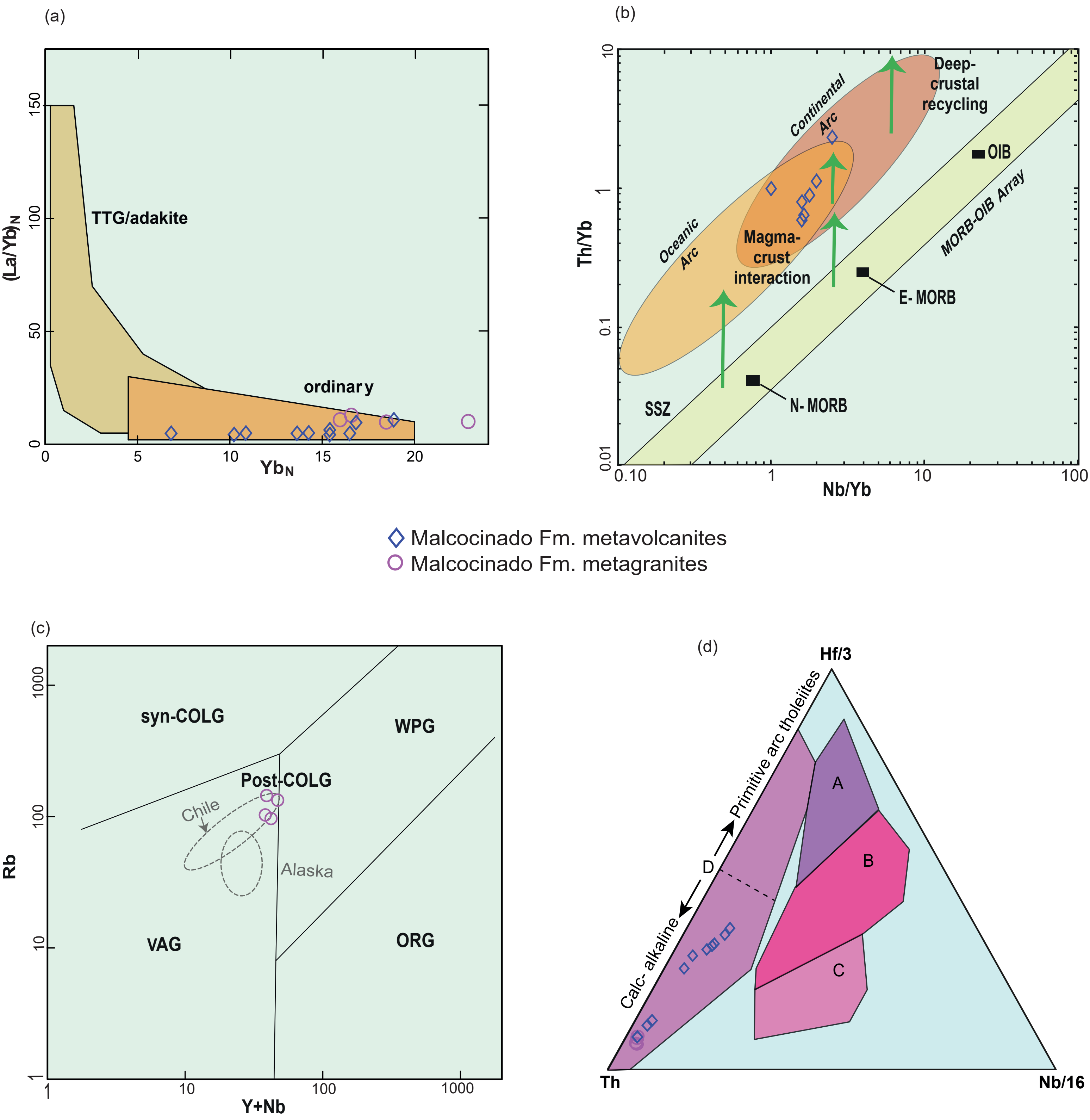

(a)
TTG/adakite
ordinary
(La/Yb)N
YbN
(b)
Deep-crustal recycling
Continental Arc
Oceanic Arc
Magma-crust interaction
OIB
MORB-OIB Array
E- MORB
N- MORB
SSZ
Th/Yb
Nb/Yb
Malcocinado Fm. metavolcanites
Malcocinado Fm. metagranites
(c)
syn-COLG
WPG
Post-COLG
Chile
Alaska
VAG
ORG
Rb
Y+Nb
(d)
Hf/3
Primitive arc tholeiites
Calc- alkaline
D
A
B
C
Th
Nb/16

Fig. 7

figure

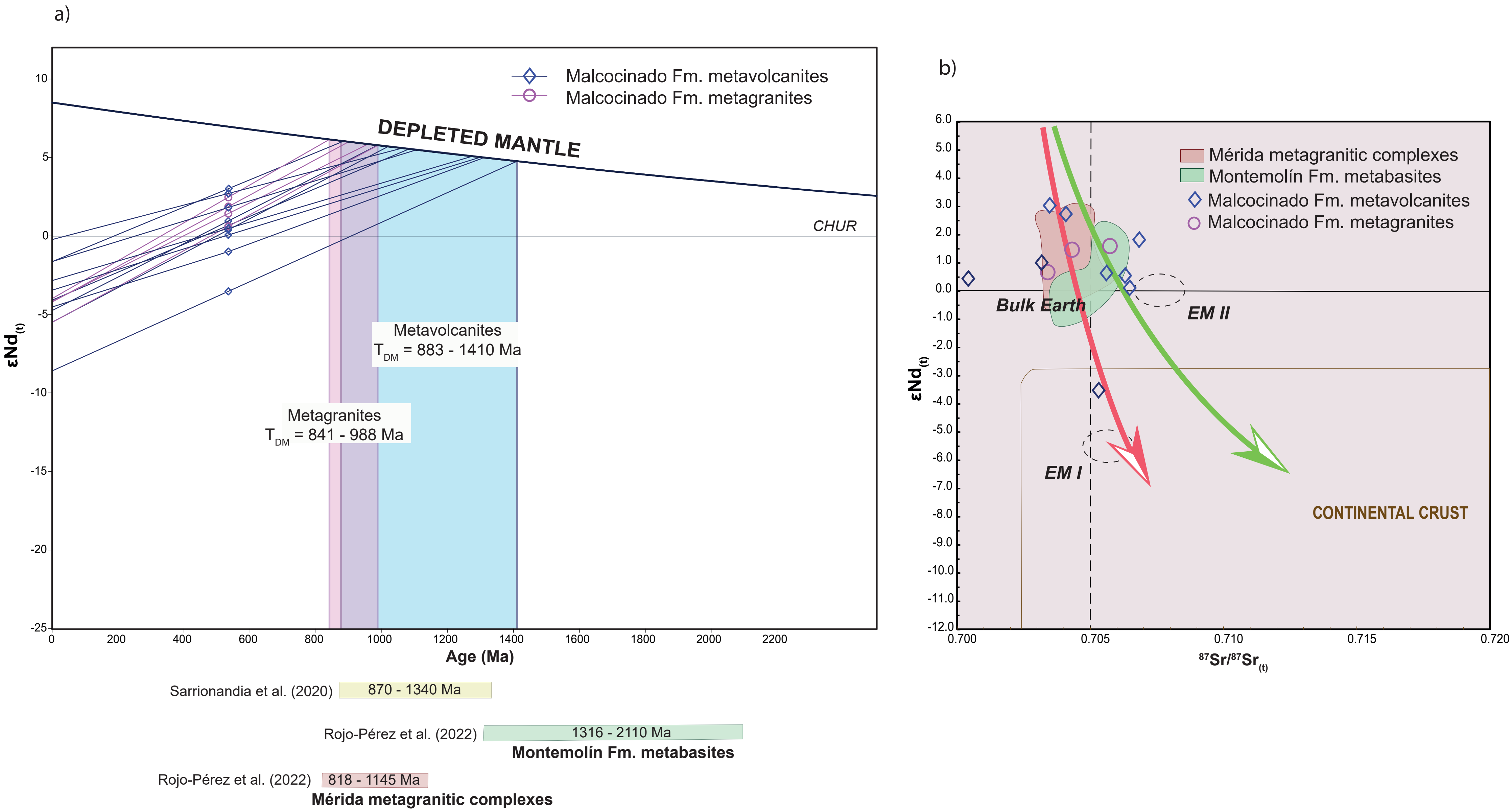

a)
Malcocinado Fm. metavolcanites
Malcocinado Fm. metagranites
DEPLETED MANTLE
CHUR
Metavolcanites
T DM = 883 - 1410 Ma
Metagranites
T DM = 841 - 988 Ma
εNd(t)
Age (Ma)
Sarrionandia et al. (2020)
870 - 1340 Ma
Rojo-Pérez et al. (2022)
1316 - 2110 Ma
Montemolín Fm. metabasites
Rojo-Pérez et al. (2022)
818 - 1145 Ma
Mérida metagranitic complexes
b)
Mérida metagranitic complexes
Montemolín Fm. metabasites
Malcocinado Fm. metavolcanites
Malcocinado Fm. metagranites
Bulk Earth
EM II
EM I
CONTINENTAL CRUST
εNd(t)
87Sr/87Sr(t)

Fig. 8

figure

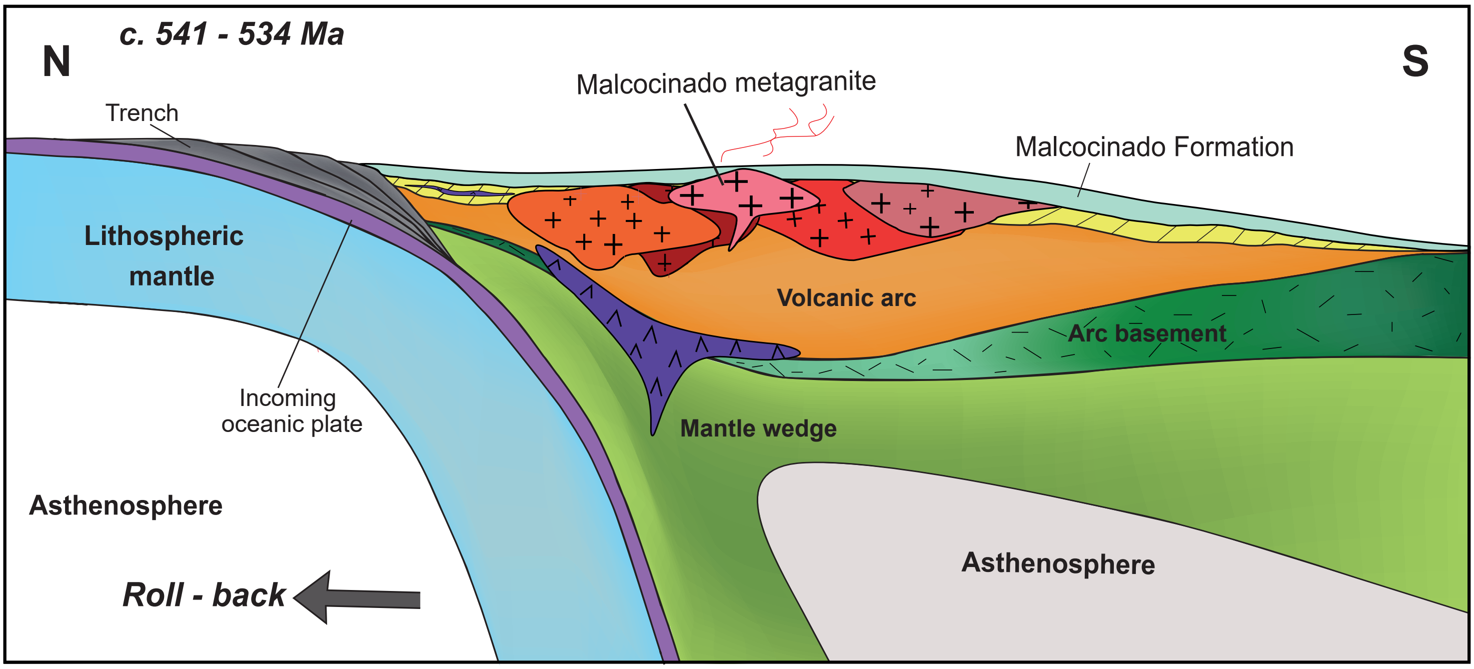

Magmatic event at c. 541 Ma
Magmatic event at c. 541 Ma
Magmatic event at c. 550 Ma
Magmatic event at c. 602 Ma
Calc-alkaline mafic magmas pre- 602 Ma
Siliciclastic series (Ediacaran Serie Negra Group)

Fig. 9